Genotype-phenotype correlations and de novo induction of cancer stem cells in Wilms tumor initiation

N.S. Pop[1], D. Koot[1,4], C.M. Brouwers[2], M.M. Linssen[2], J.W.C. Claassens[2], C.W.J. Cartlidge[3], D.D. Özdemir[3,5,6], K.S. Dolt[1,3], P. Hohenstein[1,2,3,*]

[1]Department of Human Genetics, Leiden University Medical Center, Leiden, Netherlands

[2]Transgenic Facility Leiden, Central Animal Facility, Leiden University Medical Center, Leiden, Netherlands

[3]Division of Developmental Biology, The Roslin Institute, Edinburgh, United Kingdom

[4]Present adres: European Research Institute for the Biology of Ageing, University of Groningen, University Medical Center Groningen, Groningen, The Netherlands

[5]Present adres: Koç University Research Center for Translational Medicine (KUTTAM), Istanbul, Turkey

[6]Present adres: Koç University School of Medicine, Istanbul, Turkey

* Correspondence: p.hohenstein@lumc.nl

Summary

Wilms tumor, the most common pediatric kidney cancer, arises from abnormal embryonic kidney development. Therapy resistance and tumor recurrence remain major challenges, likely driven by the presence of Cancer Stem Cells (CSCs). Here, we elucidate the earliest pathogenic events in genetically engineered mouse models exhibiting loss of *Wt1* or *LIN28B* overexpression, two Wilms tumor driver genes. Loss of *Wt1* leads to a disturbance of lineage identity of the mutant cells, whereas LIN28B leads to a disturbed transition between uninduced and induced NPC (nephron progenitor cell) state. In both cases the appearance of cells positive for all four Wilms tumor cancer stem cell markers is the result of the tumor initiating mutation. The existence of genotype-phenotype correlations in primary developmental phenotypes and cancer stem cell expression patterns has important implications for therapeutic opportunities and requirements.

Introduction

Wilms tumor is the most common pediatric renal malignancy, occurring in approximately 1 in 10,000 children, typically before the age of five (Spreafico et al., 2021). They arise from aberrant embryonic kidney development, potentially during the critical window of definitive kidney development between the fifth and eight week of gestation (Zheng et al., 2023). Standardized diagnostic and therapeutic procedures have made it possible to cure nearly 90% of the affected children. However, therapy resistance, postoperative recurrence, and high-risk Wilms tumors remain significant clinical challenges. Histological analyses consistently reveal persistence of embryonic renal structures within tumors (Beckwith et al., 1990; Hohenstein et al., 2015), including a subset of tumor cells resembling progenitor-like cells. These observations are consistent with the cancer stem cell (CSC) model, in which a small population of stem cell-like cells drives tumor initiation, recurrence, and therapy resistance, potentially explaining the poor outcomes observed in high-risk Wilms tumor (Bonnet and Dick, 1997; Ginestier et al., 2007; Pode-Shakked et al., 2013). Understanding the origin of these Wilms tumor CSCs would provide valuable insights in the biology of WT and the earliest pathogenic events driving Wilms tumor formation, thus providing new leads to improve patient prognosis and develop targeted therapies.

Several studies defined the Wilms tumor CSC in patient-derived material (Petrosyan et al., 2023; Pode-Shakked et al., 2013). NCAM1^{+} cells with high ALDH activity were found capable of initiating xenograft tumors, fulfilling key CSC criteria, although these cells lost tumorigenic potential when cultured *ex vivo* (Pode-Shakked et al., 2009; Pode-Shakked et al., 2013). More recently a SIX2^{+}CITED1^{+} population was described as a different kind of CSC, maintaining tumor-initiating capacity in culture and meeting the CSC criteria (Petrosyan et al., 2023).

These identified CSC markers have distinct functions during normal embryonic kidney development. Polysialylated NCAM1 (PSA-NCAM1), the embryonic version of the neural cell

52 adhesion molecule 1 (NCAM1), is an important protein that mediates cell-cell adhesion, is
53 expressed on NPCs and endothelial cells and facilitates cell movement during kidney
54 development (Niculovic et al., 2025). The protein is expressed in undifferentiated metanephric
55 mesenchyme at E11.5-E12.5 and in early nephron structures (comma- and S-shaped bodies)
56 during kidney development, but is absent postnatally (Markovic-Lipkovski et al., 2007). *Ncam1*-
57 deficient mice exhibit impaired glomerular vascularization, with reduced endothelial cell
58 numbers and smaller glomeruli, indicating an essential role for NCAM1 in kidney vascularization
59 in the mouse embryonic kidney (Niculovic et al., 2025). ALDH activity, measurable using the
60 ALDEFLUOR assay, is a widely used CSC marker (Ginestier et al., 2007). Multiple ALDH isoforms
61 contribute to this signal, including ALDH1A1, ALDH1A2, ALDH1A3 and ALDH2 (Zhou et al., 2019).
62 ALDH enzymes synthesize retinoic acid from retinaldehyde, a critical signaling molecule that
63 regulates cell differentiation, proliferation, and tissue patterning (Niederreither et al., 1999).
64 Expression is lineage- and stage-specific: *Aldh1a1* and *Aldh1a3* are dynamically expressed in
65 differentiating tubular structures derived from the nephrogenic lineage or ureteric bud, whereas
66 *Aldh1a2* is mainly localized in the cortical stroma and essential for ureteric bud outgrowth and
67 nephron formation, and is weakly expressed in the early nephron (comma- and S-shaped bodies,
68 and in the glomerulus) (Li et al., 2020; Li et al., 2017).

69 Transcription factors *Six2* and *Cited1* mark uninduced NCPs (Kobayashi et al., 2008;
70 Mugford et al., 2009). Upon NPCs induction, *Cited1* expression is lost first, followed by *Six2*
71 (Mugford et al., 2009). The persistence of SIX2^{+}CITED1^{+} populations in Wilms tumor xenografts
72 suggests that these tumors may originate from nephron progenitors that failed to undergo proper
73 differentiation, although this developmental process has yet to be conclusively demonstrated.
74 The normal expression pattern of these CSC markers suggest that NCAM1^{+}ALDH-activity is a
75 natural occurrence in early nephron structures (comma- and S-shaped bodies), whereas
76 SIX2^{+}CITED1^{+} reflects a transcriptional signature of uninduced NPCs.

77 To date, 46 Wilms tumor predisposition and driver genes have been identified, many of
78 which are essential for embryonic kidney development and are classified in different functional
79 groups (Spreafico et al., 2021). Most existing data on biological aspects of Wilms tumors was
80 obtained without knowing the mutational status of Wilms tumor genes in the samples and it is
81 therefore unclear how universally applicable the findings are for any given Wilms tumor. The
82 different functional classifications of Wilms tumor genes might lead to different underlying
83 biology of tumors with different mutations, and if so, different opportunities or requirements for
84 therapeutic intervention. It will also affect the outcome of clinical trials if the patients are not
85 properly matched to the treatment that is being tested. Even if full genome sequencing of Wilms
86 tumor samples would become routine, without understanding what biological effects different
87 mutations have this will remain a major obstacle to further improving Wilms tumor patient
88 outcome.

89 Wilms Tumor 1 (*WT1*) is the most extensively studied Wilms tumor gene. Although best
90 known as a transcription factor, WT1 can bind both RNA and DNA, functioning as either an
91 activator or repressor depending on the cellular and chromatin context or in RNA metabolism
92 (Essafi et al., 2011; Hohenstein and Hastie, 2006). Although best known as a transcription factor,
93 WT1 can bind both RNA and DNA, functioning as either an activator or repressor depending on
94 the cellular and chromatin context or in RNA metabolism (Essafi et al., 2011; Hohenstein and
95 Hastie, 2006). During nephrogenesis, WT1 is critical for driving mesenchymal-to-epithelial
96 transition (MET) in NPCs. Approximately 15% of patients carry loss-of-function *WT1* mutations,
97 which are frequently associated with ectopic tissue differentiation into skeletal muscle, fat, and
98 less commonly bone or cartilage (Miyagawa et al., 1998; Schumacher et al., 2003).

99 Another Wilms tumor driver gene, *LIN28B*, is primarily expressed in progenitor cells,
100 where it promotes proliferation and blocks differentiation by inhibiting maturation of the let-7
101 microRNAs, thereby upregulating oncogenic targets including *RAS*, *MYC*, and *HMGA2*
102 (Viswanathan and Daley, 2010). LIN28B has been implicated in tumor progression, epithelial-to-

103 mesenchymal transition, CSC formation, and therapy resistance (Cotino-Najera et al., 2024; Li
104 et al., 2019; Zhou et al., 2013). Its precise role in kidney development is unclear, its declining
105 expression by embryonic day (E)16.5 suggests a temporally restricted function during
106 nephrogenesis (Viswanathan and Daley, 2010; Yermalovich et al., 2019). The earliest phenotypic
107 events following *WT1* loss or *LIN28B* overexpression in Wilms tumor patients remain largely
108 unknown, limiting our understanding of how these mutations initiate tumorigenesis.

109 Genetically engineered mouse models provide a powerful model to study the earliest
110 phenotypic effects of tumor-initiating mutations in a controlled developmental context. These
111 models allow us to study the direct consequences of Wilms tumor-initiating mutations and track
112 emergence, expansion, and expression of cell populations that could act as CSCs. Here we use
113 lineage specific loss of *Wt1* and *LIN28B* overexpression mouse models to study the genotype-
114 phenotype correlations during kidney development, and their effects on CSC marker expression.

Results

Conditional Wt1 knockout models

We previously knocked out *Wt1* at different stages of nephron development using *Nes*-Cre, *Pax8*-Cre a *Wnt4*-Cre drivers, showing that the earliest, pre-MET loss of *Wt1* using *Nes*-Cre most closely resembled *WT1*-mutant tumors. It led to an expansion of mesenchyme and a block of MET (Berry et al., 2015). The metanephric mesenchyme gives rise to the condensed mesenchyme containing the nephron progenitor cells (NPCs), expressing *Six2* (Kobayashi et al., 2008), and the remaining uncondensed mesenchyme containing stromal progenitor cells with a distinct expression pattern of *Foxd1* (Kobayashi et al., 2014). Both populations transiently express *Wt1* (Armstrong et al., 1993; Berry et al., 2015; Weiss et al., 2020). The *Nes*-Cre model affects both lineages, and therefore cannot distinguish between the roles of *Wt1* in them. To determine the nephrogenic- and stromal-specific effects when *Wt1* is lost, we used three Cre-drivers: *Six2*$^{\text{GFPCre-IRES-PuroR}}$ (*Six2*^{GCiP}) to target the nephrogenic lineage, *Foxd1*^{GFPCre} (*Foxd1*^{GC}) to target the stromal lineage, and *Wt1*$^{\text{CreERT2}}$ (*Wt1*^{CE}) for targeting both lineages in a tamoxifen-dependent controlled manner (Dolt et al., 2013; Kobayashi et al., 2014; Zhou et al., 2008). We crossed the three Cre-drivers with the *Wt1* conditional allele (Martinez-Estrada et al., 2010) and in some cases included the lox-stop-lox tdTomato reporter (Madisen et al., 2010) to follow the lineage of mutant and control cells. This conditional *Wt1* knockout model is a phenocopy of the conventional model (Kreidberg et al., 1993) when driven by a germline Cre deleter strain, and does not have a phenotype when driven by the *Hoxb7*-Cre ureteric bud-specific driver (Berry et al., 2015).

137 ## *Six2*-driven Wt1 loss blocks nephrogenesis

138 To selectively delete *Wt1* in the nephrogenic lineage, we used the *Six2*^{GCiP} driver to knockout *Wt1*
139 in the developing kidney (Fig. 1A). *Six2* is expressed in NPCs from E10.5 in the metanephric
140 mesenchyme and later in the cap mesenchyme, and is predicted to be a direct transcriptional
141 target of *Wt1* (Kobayashi et al., 2008; O'Brien et al., 2018). As NPCs form pretubular aggregates
142 (PTA), which epithelializes into a renal vesicles (RV), comma-shaped and S-shaped bodies to
143 form a mature nephron (McMahon, 2016), *Six2* expression is lost.

144 *Ex vivo* kidney organ culture time lapse imaging of the *Six2*^{GCiP} allele (Dolt et al., 2013) in
145 control E12.5 embryonic kidneys confirmed *Six2*-linked GFP expression in the cap mesenchyme,
146 and the tdTomato lineage reporter confirmed contribution to the nephrogenic lineage, with
147 exclusion from the stroma and ureteric bud (Fig. 1B, left panel; supplementary movie 1A). In
148 contrast, e*x vivo* kidney organ cultures of E12.5 *Six2*^{GCiP} driven *Wt1*-mutant kidneys showed
149 severely disrupted nephron differentiation and ureteric bud branching morphogenesis (Fig. 1B,
150 right panel; supplementary movie 1B). At 0hrs, the *Wt1*-mutant eGFP expressing cells
151 surrounded the ureteric bud tip, but subsequently the eGFP signal decreased, indicative of cells
152 losing SIX2-expression, consistent with *Six2* as potential *Wt1* target (O'Brien et al., 2018). The
153 tdTomato-expressing mutant cells accumulated around the ureteric bud tip, or migrated rapidly
154 outwards. Whole mount immunohistochemical staining confirmed loss of SIX2 in the tdTomato-
155 expressing cells (Fig. 1C).

156 Consistent with the time lapse imaging, histological analysis of E12.5 embryos showed
157 ureteric bud tips surrounded by mesenchymal-like cells (Fig. 1D). Immunohistochemistry
158 confirmed loss of SIX2 expression in tdTomato-expressing cells (Fig. 1E, top panels), which had
159 lost WT1 expression and surrounded a CDH1-positive tubular structure (Fig. 1E, bottom panels).
160 Surrounding stroma, negative for tdTomato, continued to express WT1. Proliferative marker KI67
161 is reduced in the kidney region (Sup. Fig. 5A-B).

162 At E18.5, mutants exhibited structures resembling early budding stage. Sectioning the
163 isolated urogenital system complicated the identification of the kidney remnants in 2D, due to
164 their lower localization in the embryo (Fig. 1F, arrows). The derived structures were negative for
165 SIX2, WT1, and CDH1 expression, making it difficult to define their developmental stage, cellular
166 identity, or structural nature. Nevertheless, these structures were located in the anatomical
167 region where kidneys are expected to form.

168

169 ## *Foxd1*-driven Wt1 loss disrupts ureteric bud branching and cortical organization

170 We used the *Foxd1*^{GC} driver (Kobayashi et al., 2014) to delete *Wt1* specifically in FOXD1^{+} stromal
171 progenitors (Fig. 2A). The FOXD1^{+} stromal progenitors originate from the uncondensed
172 mesenchyme and are first present around E11.0, when they begin populating the cortical and
173 medullary interstitium, the fibrocytes of the capsular tissue and the vascular-supporting
174 pericytes (Kobayashi et al., 2014).

175 Lineage tracing of *Foxd1*^{GC} through tdTomato expression in *ex vivo* control kidney organ
176 cultures confirmed expression in the stromal lineage surrounding the nephrogenic caps and
177 branched ureteric bud (Fig. 2B, left panel; supplementary movie 2A). In contrast, *ex vivo* organ
178 cultures of *Foxd1*^{GC} driven *Wt1*-mutant kidneys showed altered ureteric bud morphogenesis,
179 characterized by reduced branching complexity, elongated and sparser branches, increased
180 spacing between them, and fewer terminal tips (Fig. 2B-C; supplementary movie 2B) - a
181 phenotype similar to that described previously (Weiss et al., 2020). Mutant kidneys are smaller,
182 consistent with reduced branching complexity and fewer nephrogenic caps (Fig. 2D).

183 Histological analysis of E12.5 sections confirmed decreased ureteric bud branching in
184 the *Wt1*-mutants (Fig. 2E). Ureteric bud tips were surrounded by loosely organized NPCs. The
185 *Foxd1*-lineage confirmed strong contribution to the stromal compartment (Fig. 2F, upper panels).
186 We observed some SIX2^{+} tdTomato^{+} cells in the cap mesenchyme of control kidneys (Fig. 2F,

187 white arrows), though these cells expressed lower SIX2 levels compared to surrounding cap
188 mesenchymal. Such double-positive cells were absent in *Foxd1*-driven *Wt1*-mutant kidneys.
189 Antibody staining confirmed loss of WT1 in the stroma surrounding the cap mesenchyme, while
190 the cap mesenchyme itself remained WT1^{+} (Fig 2F lower panels).

191 At E18.5, mutant kidneys appeared smaller, with expanded cortical stroma between the
192 developing nephrons – consistent with the phenotype described by Weiss et al (Fig. 2G). We
193 observed disrupted nephrogenic zone organization, including SIX2^{+} caps that lost their apical
194 orientation and started moving inwards (Fig. 2H upper panels, white filled arrow; Sup. Fig. S1).
195 This may be the consequence of expansion and migration of cortical stromal cells into the
196 nephrogenic zone. We detected tdTomato^{+} cells in or around proximal tubules (LTL^{+}) (Fig. 2H,
197 white open arrows). It is not clear if these cells are part of the proximal tubules. Staining for WT1
198 in control kidneys at E18.5 showed low expression in the stroma, which was absent in mutants
199 (Fig. 2H lower panels). Proliferative marker KI67 is highly expressed in the nephrogenic zone,
200 comparable to the control kidneys (Sup. Fig. 5A-B).

201

202 Combined nephrogenic and stromal Wt1 loss delays kidney development and initiates
203 blastemal features

204 Targeting the nephrogenic lineage alone caused a severe developmental block, whereas
205 targeting the stromal lineage led to stromal overgrowth, nephrogenic delay, and altered ureteric
206 bud morphogenesis, but each was different form the *Nes*-Cre driven *Wt1* knockout (Berry et al.,
207 2015). Since *Wt1* is expressed in both lineages we combined the conditional *Wt1* knockout and
208 tdTomato reporter alleles with the *Wt1*^{CE} knock-in driver (Zhou et al., 2008). The latter is itself a
209 *Wt1*-inactivating allele, so in the tamoxifen induced embryos the Cre-induced loss of the
210 conditional *Wt1* copy results in complete loss of the protein (Fig. 3A). To determine the best
211 window and dosage for targeting the SIX2^{+} nephrogenic lineage and surrounding stroma, we

212 tested single dose Tamoxifen (Tx) injections at E8.5, E9.5, E10.5 or E11.5, on embryonic reporter
213 kidneys isolated at E12.5 and *ex vivo* cultured the kidneys from the treated litters for 48-72hrs.
214 The tdTomato signal indicated the lineage of cells where recombination happened (Fig. 3B).
215 Single Tx injections targeted most of the cells of both lineages when injected at E9.5 or E10.5.
216 Double injections at E9.5 and E10.5 increased this number of targeted cells in the nephrogenic
217 zone. Immunostaining for SIX2 expression showed some cells that lacked tdTomato expression,
218 indicating incomplete Cre activity (Fig. 3B, white arrows). This observation of "escaping"-cells is
219 similar to what has been described for the *Nes*-Cre driven *Wt1* conditional knockout model (Berry
220 et al., 2015) although in the current case it is likely due to incomplete activation of the
221 recombinase by tamoxifen.

222 We used the double E9.5+E10.5 Tx treatment to knockout *Wt1*. We compared mutant
223 kidneys to littermate controls which lacked the CreERT2 allele, but were equally exposed to Tx.
224 In this case the control samples lack Cre activity and will therefore not activate the tdTomato Cre
225 reporter. Lineage tracing of *Wt1*-mutant kidneys revealed smaller kidneys with altered ureteric
226 bud branching and fewer nephrogenic caps (Fig. 3C; supplementary movie 3A-B), similar to the
227 *Foxd1*^{GC} driven mutants. The morphology of the cells suggested that mutant cap mesenchymes
228 lacked epithelialization (Fig. 3C, white arrows), a sign of delayed or blocked MET, a process in
229 which we showed WT1 plays a key role before (Berry et al., 2015; Davies et al., 2004; Essafi et al.,
230 2011).

231 Histological assessment at E12.5 showed a thinner NPC layer in mutants compared to
232 controls (Fig. 3D). The NPC population is dispersed, lacking the tight cap-like structure around
233 the ureteric bud tips. The ureteric bud epithelium appears less branched compared to the
234 control. The stroma in the control is relatively thin and confined around the nephrogenic zone,
235 where in the mutant it appears to be expanded – more stroma surrounding the ureteric bud tips
236 and nephron progenitors. The stroma is less organized and seems loosely packed.

237 Immunohistochemistry for SIX2 and tdTomato confirmed incomplete Cre activation in mutants,
238 evidenced by SIX2^{+} tdTomato^{-} cells (Fig. 3E, white arrows), while controls lacked CreERT2 and
239 were tdTomato^{-} (data not shown). Co-staining for SIX2 and WT1 revealed double-positive cells,
240 the "escaping" SIX2^{+} tdTomato^{-} cells (Fig. 3E lower panels). CDH1 staining further supported the
241 presence of widened, misshaped epithelium (Fig. 3E lower panels).

242 Mutant kidneys at E18.5 were markedly smaller, lacked clear corticomedullary
243 segmentation, and displayed severely altered nephrogenesis, with only a few glomeruli present
244 (Fig. 3F). Embryonic-like epithelium was observed in the nephrogenic zone, with emerging
245 blastemal-like regions (Fig. 3F). Staining for proliferative mark KI67 reveals disorganized
246 expression of the protein, with high expression observed in the cortical-region (Sup. Fig. 5B white
247 arrows). Stromal overgrowth was also evident. WT1 immunohistochemistry revealed "escaping"
248 nephrons (Fig. 3G), consistent with observations at E12.5. Mutant kidneys displayed reduced
249 LTL^{+} proximal tubules, consistent with impairment of MET and blocked or delayed nephron
250 differentiation (Fig. 3G).

251

252 ALDH1A2 is the primary contributor to ALDEFLUOR activity in Wilms tumour CSCs

253 Wilms tumor blastema is associated with the Wilms tumor Cancer Stem Cells (CSCs). As
254 mentioned above, the two sets of Wilms tumor CSC markers (NCAM1^{+} with ALDEFLUOR-activity
255 (Pode-Shakked et al., 2013), and SIX2^{+}CITED1^{+} (Murphy et al., 2012; Petrosyan et al., 2023)) are
256 both linked to tumor maintenance and progression. In the first marker set, ALDH activity was
257 measured using the ALDEFLUOR assay, which requires living cells, analyzed through flow
258 cytometry. To investigate whether similar NCAM1/ALDH patterns occur during kidney
259 development, we repeated the NCAM1/ALDERED assay (analogous to ALDEFLUOR) on
260 embryonic mouse kidneys. No significant differences were observed between mutant and
261 control kidneys for all lineage-specific *Wt1* mutant kidneys (Sup. Fig. 2).

262 To visualize the protein expression levels of the CSC markers over the course of
263 embryonic kidney development, we first determined which ALDH-paralogue was the primary
264 contributor to the ALDEFLUOR assay in WT patient samples. ALDH1A1, ALDH1A2, ALDH1A3 and
265 ALDH2 can all contribute to the detected signal (Zhou et al., 2019). In the context of Wilms tumor,
266 ALDH1A2 has been suggested to be the paralogue associated with CSCs (Petrosyan et al., 2023;
267 Wegert et al., 2020), but its specificity for Wilms tumors has not yet been proven. We reanalyzed
268 microarray data (Shukrun et al., 2014) from Wilms tumor xenograft fractions unsorted and sorted
269 for NCAM1^{+}ALDEFLUOR^{+} and NCAM1^{+}ALDEFLUOR^{-} (Sup. Fig. 3A). The NCAM1+/ALDEFLUOR+
270 fraction shows high expression for both *ALDH1A2* and *ALDH1A3*. Nonetheless, *ALDH1A3*
271 expression is not enriched in the CSC fraction given its higher expression in the unsorted fraction.
272 *ALDH1A1* is low in all fractions and *ALDH2* is high in unsorted and decreased in both sorted
273 fractions. *ALDH1A2* is the only paralogue specifically upregulated in the NCAM1+/ALDEFLUOR+
274 faction and therefore these results indicate that ALDH1A2 is the principal contributor to the
275 ALDEFLUOR activity in these Wilms tumor CSCs.

276 To examine ALDH1A-paralogue expression in the developing mouse kidney, E12.5
277 embryonic kidneys were cultured *ex vivo* for 24, 48 and 72 hours and stained for ALDH1A1,
278 ALDH1A2, and ALDH1A3. ALDH1A1and ALDH1A3 were weakly detected in the ureteric bud
279 epithelium, whereas ALDH1A2 showed strong expression in the cortical region of the kidney, in
280 close proximity of the nephrogenic caps, presumably marking stromal cells (Sup. Fig. 3B). Only
281 in the E12.5 kidneys cultured for 48hrs weak ALDH1A2 expression was observed in renal vesicle-
282 shaped structures. Co-staining with FOXD1 antibodies confirmed the stromal identity of the
283 ALDH1A2 positive cells. These findings support ALDH1A2 is mainly localized to the cortical
284 stroma, with weaker protein expression patterns in the epithelializing nephron (Sup. Fig. 3C).

285

286 ## CSC Marker sets for committed and uncommitted NPCs

287 The CSC marker sets were identified on xenograft derived tumor tissues (Petrosyan et al., 2023;
288 Pode-Shakked et al., 2013), which might not reflect the developmental stage of origin anymore.
289 To map these CSC markers onto normal developing kidneys and examine their dynamics in the
290 context of Wilms tumor mutations, we performed immunohistochemistry for NCAM1, ALDH1A2,
291 SIX2, and CITED1 in embryonic kidneys from control and *Wt1*-mutants at E12.5 and E18.5. Due
292 to overlapping antibody host species, ALDH1A2 and CITED1 were analyzed on consecutive
293 sections, resulting in two staining combinations: (NCAM1, ALDH1A2, SIX2; and NCAM1, CITED1,
294 SIX2.

295 In normal embryonic kidneys, NCAM1^{+}ALDH1A2^{+}SIX2^{+} triple-positive cells localized to
296 the SIX2^{+}CITED1^{-} committed NPC/PTA population (Fig. 4A, upper panels, white arrows). These
297 committed NPC/PTA cells exhibited low ALDH1A2 expression compared to surrounding stromal
298 cells. In contrast, the uninduced SIX2^{+}CITED1^{+} cells co-express NCAM1, while they lack
299 ALDH1A2 expression, defining a more uninduced NCAM1^{+}CITED1^{+}SIX2^{+} population (Fig. 4 A,
300 lower panels). Therefore, in normal developing kidneys ALDH1A2 and CITED1 display a mutually
301 exclusive expression pattern. Early nephron structures such as comma- and S-shaped bodies
302 strongly expressed NCAM1 and ALDH1A2 but lacked SIX2 and CITED1, consistent with
303 expression patterns in other studies (Li et al., 2020; Li et al., 2017; Markovic-Lipkovski et al.,
304 2007).

305 Lineage-specific *Wt1* loss revealed distinct effects on these populations. *Six2*^{GCiP}-driven
306 *Wt1* mutants at E12.5 showed a reduction in NCAM1, CITED1, and SIX2 expression, while
307 ALDH1A2 expression was observed in the same region where *Wt1* was lost (Fig. 4B upper panels,
308 Fig. 2E). This suggests that *Wt1*-deficient cells obtained an alternative identity, possibly
309 differentiating towards stroma which is characterized by ALDH1A2 expression but not the other
310 markers. At E18.5, the kidney remnants showed a distinct expression pattern as observed at

311 E12.5. The kidney remnant represents a homogenous tissue structure where NCAM1 is
312 expressed, ALDH1A2 is high in the nucleus, SIX2 is low and CITED1 is lowly expressed in the
313 nucleus (Fig. 4B, lower panels). *Foxd1*^{GC} driven *Wt1* mutants resembled controls, without
314 changed CSC marker expression at E12.5 (Fig. 4C). However, we do observe a decline in
315 ALDH1A2 expression at E18.5 (Fig. 4C). In the *Wt1*^{CE} mutant model, at E12.5
316 NCAM1^{+}ALDH1A2^{+}SIX2^{+} triple-positive cells localized to the committed NPCs/PTA similar to
317 controls (Fig. 4D upper panel). By E18.5, ALDH1A2^{+} regions expanded substantially, likely
318 reflecting increased stromal content, whereas NCAM1^{+}ALDH1A2^{+}SIX2^{+} triple-positive
319 committed NPCs/PTA were scarce, consistent with impaired MET (Fig. 4D). The
320 NCAM1^{+}CITED1^{+}SIX2^{+} uninduced NPC population was present at E12.5, with CITED1 also
321 observed in the committed NPCs/PTA (Fig. 4D lower panels, white arrow), demonstrating CITED1
322 retention beyond the uncommitted NPC stage. We cannot test directly if these triple-positive
323 committed NPCs/PTA co-express ALDH1A2 due to the overlapping antibody species, but
324 ALDH1A2 expression in similar structures was observed (Fig. 4D upper panels). By E18.5, the
325 disorganized nephrogenic zone co-expressed NCAM1^{+}CITED1^{+}SIX2^{+} in the caps, in line with
326 observations in the control kidneys (Fig. 4.D lower panel) representing ALDH1A2^{-} uninduced
327 NPCs.
328

329 LIN28B-overexpression induces developmental disorganization and early Wilms tumor
330 blastema

331 To compare the lineage-specific *Wt1* loss phenotype and WT CSC marker behavior to other
332 Wilms tumor mutations, we examined the effects of LIN28B overexpression on kidney
333 development using the doxycycline (dox)-inducible model (Urbach et al., 2014). We used the
334 same *Wt1*^{GC} driver used by Urbach et al. to control lineage-specificity of the model, but added an
335 additional *lgs7*$^{TRE\text{-}LSL\text{-}tdTomato}$ allele (Madisen et al., 2015) to express a tdTomato reporter to identify
336 lineage-specific dox-induced cells (Fig. 5A). Doxycycline was provided from beginning of

337 gestation (E0). *Ex vivo* kidney organ cultures of control littermates lacked the *Wt1*^{GC} allele but
338 were exposed to doxycycline throughout gestation and *ex vivo* culturing, and showed a normal
339 developing embryonic kidney without the reporter because of the lack of the Cre allele (Fig. 5B,
340 upper panel; supplementary movie 4A). Lineage tracing of the mutant kidneys in organ cultures
341 confirmed dox induced tdTomato expression, thus LIN28B overexpression, in the three lineages
342 of the developing kidney (Fig. 5B, lower panels). The tdTomato signal was particularly strong in
343 the ureteric bud, while to lesser extend in the nephrogenic and stromal cells. Mutant kidneys in
344 organ cultures exhibited enlarged nephrogenic caps and delayed epithelialization based on the
345 morphology of the cells, identified at E12.5 + 72 hours of kidney culture (Fig. 5B; supplementary
346 movie 4B).

347 Histological analysis of LIN28B mutants at E12.5 showed the first signs of delayed
348 nephrogenesis with fewer renal vesicle-like structures and disorganized epithelium, and
349 increased stroma between the caps (Fig. 5C, left panel). By E18.5, mutant kidneys displayed
350 disorganized caps and surface indentations (Fig. 5C, right panel, orange arrows). The mutant
351 kidney exhibited regions where normal nephrogenesis occurred, alternated with blastemal-like
352 regions (Fig. 5C, red arrows and circles). These blastemal-like regions surrounding a tubular
353 CDH1^{+} structure are possibly NPCs surrounding a ureteric bud tip that turned inwards, possibly
354 explaining the observed indentations. Staining for SIX2 expression revealed that surface
355 indentations are lined by SIX2^{+} caps turning inwards (Fig. 5D, lower panel). Morphologically this
356 is suggestive for lobe formation, a phenomenon observed in human kidney development but not
357 in mice. At E12.5, WT1 expression is low in the mutant compared to control. While at E18.5 the
358 expression pattern is similar to control, but the caps are enlarged (Fig. 5D).

359 The lobes observed at E18.5 were lost by postnatal day 19 (P19). At P19, the cortico-
360 medullary segmentation disappeared, and the abnormalities in mutant kidneys developed into
361 regions where immature embryonal-appearing epithelium was accompanied by small areas of

362 blastema and stroma, potentially representing beginning Wilms tumors (Fig. 5E). These
363 blastemal-like regions co-expressed SIX2 and WT1, surrounding CDH1^{+} embryonal-appearing
364 epithelium, possibly resembling embryonic cap mesenchymes (Fig. 5F). The SIX2^{+} blastemal-like
365 regions exhibited expression patterns similar to committed NPCs, with gradual decline of SIX2
366 expression while WT1 remained robustly expressed (Fig. 5F, white arrows). The regions that lost
367 SIX2 appeared to be capable of progressing into RV-like shapes (Fig. 5F, orange arrows).

368

369 ## LIN28B-overexpression preserves embryonic marker profiles postnatally

370 We repeated the NCAM1/ALDERED assay on embryonic kidneys from the LIN28 model, but again
371 no significant differences were observed between mutant and control kidneys (Sup. Fig. 4).
372 Visualization of the four CSC protein markers revealed that the NCAM1^{+}ALDH1A2^{+}SIX2^{+}
373 committed NPCs/PTA were absent in the mutant kidneys at E12.5, consistent with delayed
374 nephrogenesis (Fig 6A upper panels). NCAM1^{+}ALDH1A2^{+} epithelialized structures, similar to
375 RV/comma- and S-shaped bodies, lacked SIX2 expression (Fig. 6A, white arrows). We observed
376 NCAM1^{+}CITED1^{+}SIX2^{+} committed NPCs/RVs (Fig. 6A lower panels, white arrows), similar as
377 described for the *Wt1*^{CE} *Wt1* mutant kidneys. By E18.5, NCAM1^{+}ALDH1A2^{+}SIX2^{+} triple-positive
378 cells were detected within the nephrogenic zone in close proximity to the indentations (Fig. 6B,
379 upper panel, white arrow). Their expression pattern resembles committed NPCs/PTA, but their
380 spatial localization differed from that of canonical NPCs/PTAs within the nephrogenic niche. The
381 observed positioning implies that these cells may have been captured in a state, potentially
382 representing the earliest stages of blastema formation, rather than undergo nephron
383 differentiation. This same blastemal-like population of cells co-expressed NCAM1^{+}CITED1^{+}SIX2^{+}
384 in consecutive sections, suggesting all four CSC makers are co-expressed in the same cells in
385 this early blastemal-like population (Fig. 6B lower panels, white arrows).

386 By P19, blastemal regions which we previously showed were positive for SIX2 and WT1 (Fig. 5F)
387 exhibited robust expression of NCAM1, ALDH1A2, CITED1, and SIX2, shown on consecutive
388 sections (Fig. 6C). Co-staining of consecutive sections demonstrated specific expression
389 patterns for ALDH1A2 and CITED1, with differential expression patterns for each in distinct parts
390 of the blastema (Fig. 6C, green arrow: high ALDH1A2, orange arrow: high CITED1, asterisk: both
391 proteins expressed). This suggests that the blastemal-like population is a heterogenous
392 population of cells, possibly reflecting uninduced NPC state when CITED1^{high}ALDH1A2^{low}, and
393 induced NPC state when CITED1^{low}ALDH1A2^{high}. We found a third population which is quadruple-
394 positive for all markers (Fig. 6C asterisks), and this could represent a transitional state between
395 uninduced and induced blastema, which is only present in the mutant. Blastemal populations
396 surrounded embryonic-like tubular structures, potentially remnants of UB tips. This is similar to
397 the phenotype described by Urbach et al. (2014), who claim that these blastema structures are
398 remains of cap mesenchymes, and that these structures are capable of differentiating into
399 nephrogenic structures in the presence of *Wnt4* (Urbach et al., 2014). These blastemal cells
400 remained proliferative, as evidenced by KI67 expression (Sup. Fig. 5).

401 ## Discussion

402 Due to the early embryonic origin of Wilms tumors, little is known about the earliest phenotypic
403 changes following tumor-initiating mutations. Genetically engineered mouse models provide a
404 unique and powerful model to study these effects in a controlled and well-understood
405 developmental context. Here we present an extensive characterization of the early events after
406 Wilms tumor mutation induction in mouse models, which shows two patient-based Wilms
407 tumor-initiating mutations result in fundamentally different changes to the developing kidney,
408 and therefore different biology underlying tumors that eventually will both be classified as Wilms
409 tumors.

410 We use the two previously described CSC marker sets as starting point for the detailed
411 analysis of the direct effects of two different Wilms tumor-initiating mutations in mouse models.
412 To enable the analysis of the Aldefluor signal using antibodies we identified ALDH1A2 as the
413 ALDH paralogue responsible for its activity in WT CSCs (Pode-Shakked et al., 2013).(Pode-
414 Shakked et al., 2013). Combining ALDH1A2 expression with the other WT CSC markers NCAM1,
415 SIX2 and CITED1 we demonstrate in normal developing mouse kidneys a succession of different
416 marker combinations in the nephrogenic lineage (Fig. 7A). An NCAM1/CITED1/SIX2 triple-positive
417 stage in uninduced NPCs is followed by a NCAM1/ALDH1A2/SIX2-positive state in induced
418 NPCs. As cells are epithelializing through the PTA and RV stages, SIX2 expression decreases,
419 until only NCAM1 and ALDH1A2 remain in the comma- and S-shaped bodies. The stromal lineage
420 is only positive for ALDH1A2 (Fig. 7A). This pattern shows that in the normal developing kidney
421 cells are either positive for the SIX2/CITED1 CSC markers (uninduced NPCs) or the other marker
422 set NCAM1/ALDH1A2 (comma-/S-shaped bodies) but not both. This means that either the two
423 CSC marker sets identify different CSCs or the Wilms tumor initiating mutations force a change
424 in CSC marker expression and induces the existence of the true Wilms tumor CSC.

425 The effect of *Wt1* loss depends on the lineage(s) where the mutation is induced. When
426 *Wt1* was lost in the nephrogenic lineage using the *Six2*^{GC} driver we observed a very severe block
427 in nephron formation, and instead a retention or even increase of mesenchymal appearance and
428 behavior of the mutant cells (Fig. 7B). ALDH1A2 is the only CSC marker found in the mutant cells,
429 which are derived from Six2^{+} cells as shown by the tdTomato-positive lineage and therefore from
430 the nephrogenic lineage. In normal developing kidneys ALDH1A2 expression in the nephrogenic
431 lineage is only found together with NCAM1, and in the absence of SIX2 only in the post-MET
432 stages. The mutant kidneys do not reach this stage, so this is unlikely to explain the observed
433 CSC marker expression. Instead, ALDH1A2^{+}-only cells are a characteristic of the stromal lineage.
434 We propose that loss of WT1 at the earliest SIX2-positive stage in the nephrogenic lineage result
435 in a developmental shift from nephrogenic to stromal lineage, which we refer to as 'lineage
436 confusion'. A precedent for this is found in the *Six2*-Cre driven loss of *Pax2* which shows a
437 comparable nephrogenic-to-stromal shift (Naiman et al., 2017).

438 Our analysis of stromal-specific loss of *Wt1* using the *Foxd1*^{GC} driver confirmed a
439 previously described phenotype for this model (Fig. 7C; Weiss et al., 2020).(Fig. 7C; Weiss et al.,
440 2020). This includes a branching phenotype in the ureteric bud and increased stroma in the
441 nephrogenic zone. No changes in the expression pattern of the CSC markers was found. We
442 found SIX2^{+} caps were occasionally displaced inward, raising the possibility of aberrant
443 lobulation (see below). Important for the role of *WT1* as Wilms tumor gene, in this mutant no
444 changes in the CSC expression patterns were found.

445 To knockout *Wt1* in both nephrogenic and stromal lineage we empirically maximized the
446 efficiency of the *Wt1*^{CE} driver for combined effect in these two lineages. Using this to knockout
447 *Wt1* we found a complex phenotype reminiscent of the previously described for the *Nes*-Cre
448 driven *Wt1* knockout (Fig. 7D; Berry et al., 2015). This included increased stroma in the
449 nephrogenic zone, finger-like aberrant branching of the ureteric bud and escaping nephrons that

450 remain *Wt1*-positive, albeit fewer than in the *Nes*-Cre driven mutant. The stromal expansion in
451 this model is much more severe than in the stromal-only *Wt1* knockout. We propose the stromal
452 expansion found in the *Wt1*^{CE}-driven mutant is a combination of a direct effect of WT1 loss in the
453 stroma as found in the *Foxd1*^{GC}-driven mutant, with the lineage confusion in the nephrogenic
454 lineage as found in the *Six2*^{GCiP}-driven model. In the E18.5 samples of the mutant we see the
455 appearance of potential NCAM1/ALDH1A2/SIX2/CITED1 quadruple-positive cells and the first
456 signs of clusters of blastemal cells as found in Wilms tumors. Although the host antibody
457 incompatibility of the CITED1 and ALDH1A2 antibodies stops of from proving this quadruply
458 positive state, it is consistent with the hypothesis stated above that the Wilms tumor initiating
459 mutation induces the existence of the CSCs.

460 There are three non-mutually exclusive ways to explain why the nephrogenic
461 phenotype in the combined nephrogenic/stromal *Wt1* knockout is less severe than in the
462 nephrogenic-only mutant. First, we cannot determine the exact moment *Wt1* is lost in either
463 mutant. The tdTomato gives an indication for this, but for the phenotype the (unknown) stabilities
464 of existing Wt1 mRNA and protein can delay the moment the phenotype is induced. Second, in
465 the *Wt1*^{CE}-driven mutant the stromal component is also mutant. It is possible that the mutant
466 stroma gives different signals to the nephrogenic lineage than normal stroma, which can modify
467 the nephrogenic phenotype. Third, the escaping nephrons in the nephrogenic/stromal double
468 mutant could provide molecular signals that partially rescue the mutant cells of the nephrogenic
469 lineage. It is important to realize that in patients Wilms tumors also start developing in a further
470 normal embryonic kidney, suggesting such a mechanism could be relevant for the origin of Wilms
471 tumors in patients as well. The reason for the incomplete Cre activity in the *WT1*^{CE} model is not
472 clear, but the extra level of tamoxifen control might provide additional variability due to variation
473 in local exposure, biological processing of tamoxifen, and increased variation in the exact timing
474 of Cre activity that could result from this could be important here. It is clear however, as was for

475 the *Nes*-Cre driver (Berry et al., 2015) that the retention of *Wt1* expression due to incomplete Cre
476 activity is the cause of these escaping nephrons.

477 Whereas the loss of *Wt1* in the nephrogenic lineage shows clear signs of lineage
478 confusion, in which the identity of the mutant cells changes, we do not find any signs of this in
479 the LIN28B model. Instead, this model is characterized by a delay in NPC differentiation leading
480 to NPC-like blastemal clusters (Fig. 7E). It is again in these cells that we find potential
481 NCAM1/ALDH1A2/SIX2/CITED1 quadruple-positive cells, though also NCAM1/CITED1/SIX2 and
482 NCAM1/ALDH1A2/SIX2 triple positive cells. In the normal induction of NPCs there is a transition
483 from CITED1 to ALDH1A2 in NCAM1/SIX2 double positive cells, but in normal development we
484 have not found any sign of a quadruple-positive transition state. We propose that in this mutant
485 model the increased LIN28B expression leads to a fluid and reversible state between the induced
486 and non-induced NPC state and the appearance of intermediate quadruple-positive CSC marker
487 cells that show the full complement of all four CSC markers and could form the seed of the
488 tumor.

489 The signs of kidney lobulation in two of the four mutants is remarkable. The mechanism
490 driving kidney lobulation and its physiological purpose are unknown, but lobulation is normally
491 not a feature of murine kidneys. It is suggested that human kidney lobulation occurs through
492 striated cells, presumably of interstitial origin, that align along the radial axis of the kidney
493 (Lindstrom et al., 2018). This is consistent with our observation of stromal cells infiltrating the
494 nephrogenic zone, possibly "dragging" these caps to the inner parts of the cortex. Further study
495 on human lobulation is necessary to draw any further conclusions on this observation and its
496 relevance for Wilms tumors.

497 In conclusion, by focusing on two sets of Wilms tumor cancer stem cell markers in
498 different mouse models for Wilms tumor genes we find that a quadruple-positive state for all CSC
499 markers is only found in the mutant kidneys, suggesting the existence of the functional CSC is

500 induced by the tumor initiating mutation. The co-expression of CITED1 and ALDH1A2 could be
501 the minimal set of Wilms tumor CSC markers, but antibody incompatibility prevents us from
502 testing this. Moreover, we find clear differences in the effect of losing *Wt1* or activating LIN28B
503 on the developing kidney, with the former leading to a change in cell identity for the mutant cells
504 and the latter a disrupted transition in the normal nephron development cascade. A different
505 underlying biology for these two mutant situations could provide different therapeutic
506 opportunities for tumors caused by these mutations, or even require different therapeutic
507 approaches. Recognizing genotype-phenotype correlations like this are essential for maximizing
508 the chance of successful preclinical trials through selection of the right patients for the right trial.
509 Further detailed analyses of the developmental effects of other Wilms tumor mutations is
510 required to determine if the two phenotypes described here cover the full spectrum of Wilms
511 tumor biology or if additional primary phenotypes exist.

512

513 ## Methods

514

515 ### Animals

516 The animal care and experimental procedures were approved by the Animal Welfare Body Leiden
517 and are in accordance with the Dutch Experiments on Animals Act and EU Directive 2010/63/EU.
518 For timed pregnancies, males Wt1$^{tm2(cre/ERT2)Wtp}$/J, Wt1$^{tm1.2Ndha}$Six2$^{tm1(EGFP/cre)Phoh}$ and
519 Wt1$^{tm1.2Ndha}$B6;129S4-Foxd1$^{tm1(GFP/Cre)Amc}$/J were crossed with female Wt1$^{tm1.1Ndha}$ to conditionally
520 knockout Wt1. To activate the CreERT2 in the WT2 mouse, tamoxifen (Sigma: T5648) (2mg/40g
521 body weight) dissolved in corn oil (Sigma: C8267) was administered intraperitoneally. Pregnant
522 females received injections at E8.5, E9.5, E10.5, E11.5, or combined at E9.5 and E10.5. To
523 conditionally activate LIN28B, male Wt1$^{tm1(EGFP/cre)Wtp}$/J and Wt1$^{tm1(EGFP/cre)Wtp}$/J*B6.Cg-Igs7$^{tm62.1(tetO-}$
524 $^{tdTomato)Hze}$/J were crossed with female B6.Cg-Gt(ROSA)26Sor$^{tm1(rtTA*M2)Jae}$B6.Cg-Col1a1$^{tm2(tetO-}$
525 $^{LIN28B)Gqda}$. Doxycycline (Thermo Fisher Scientific, 24390-14-5) (1g/L) was provided via the drinking
526 water to the pregnant female mouse at E0. Pregnant females were euthanized by cervical
527 dislocation for collection of (embryonic) kidneys. Pups at P19 were euthanized by cervical
528 dislocation for kidney collection.

529

530 ### Ex vivo kidney organ culture

531 Embryonic kidneys were isolated from E12.5 embryos derived from the mouse model crosses
532 described above. Kidneys were dissected and placed on a Transwell polyester membrane insert
533 (0.4 µm pore size, Corning, 3450) in six-well plates. The lower chamber was filled with 1ml kidney
534 culture medium to establish an air-liquid interface. The culture medium consisted of DMEM
535 [Gibco 41966029], MEM Non-Essential Amino Acids 1x [Gibco 11140035], Penicillin-
536 Streptomycin 5U/ml [Gibco 15070063], βMeOH 50µM [Gibco 31350010] and 10% FCS, with or
537 without doxycycline (2µg/mL). Cultures were maintained at 37°C in 5% CO_2. After 1hr, when

538 kidneys had attached to the membrane, imaging was started in an on-stage incubator chamber.
539 Images were acquired every hour for 72-96 h. When finished, kidneys were fixed in 4%
540 paraformaldehyde (PFA) in 1xPBS for 20', washed 3x10' in 1xPBS, followed by whole kidney
541 immunofluorescent staining as described below.
542

543 ## Histological and immunofluorescent staining

544 Freshly isolated (embryonic) kidneys or whole embryos were fixed in 4% PFA and embedded in
545 paraffin. Smaller tissues were first embedded in 2% low-melting agarose prior to paraffin
546 embedding. 5 µm sections were made using a microtome. Slides with sections were dewaxed
547 with xylene and rehydrated through a series of washes with 100%, 95% and 80% ethanol.
548 Hematoxylin (Agilent, S330930-2) staining was performed through the following protocol: slides
549 were rinsed in deionized water, followed by 3' in hematoxylin, rinsed in deionized water, 5' under
550 running tap water, 12x dipped in acid ethanol, 2x1' in tap water, 1x2' in deionized water. For the
551 eosin (Sigma-aldrich, HT110232) stain, slides were stained for 30" in eosin solution, followed by
552 1' in 80% ethanol, 1' in 90% ethanol, 1' in 100% ethanol and 2x5' in xylene before being mounted
553 with Pertex (Histolab, 00811-EX). For immunofluorescent staining, antigen retrieval was
554 performed in 10mM sodium citrate (J.T.Baker, 6132043) buffer with 0.05% Tween-20 (Sigma
555 Aldrich, 274348) (pH 6.0) in a pressure cooker for 20'. Slides were blocked in 1x PBS with 2%
556 serum for 1hr at RT. Primary antibodies were incubated o/n at 4°C, followed by washing 3x10' in
557 1xPBS the next day. Secondary antibodies were incubated o/n at 4°C, followed by co-staining for
558 DAPI (Polysciences, 09224-10) and mounting with FluorSave reagent (Merck Millipore, 345789).
559 Primary antibodies: Wt1 (1:50; Abcam, ab89901), Six2 (1:200; Abnova, H00010736-M01), E-
560 cadherin/Cdh1 (1:200; BD Biosciences, 610182), Ncam1 (1:40; R&D systems (Bio Techne),
561 AF2408), Aldh1a2 (1:100; Abcam, ab96060), Cited1 (1:200; ThermoFisher, 26999-1-AP), LTL
562 unconjugated-biotinylated (1:400; Vector laboratories, L-1320-5), tdTomato (1:100;
563 ThermoFisher, TA150128), Ki-67 (1:200; ThermoFisher, MA5-14520). Secondary antibodies: Goat

anti-Rabbit IgG Cross-Adsorbed Secondary Antibody, Alexa Fluor 647 (1:1000; Thermofisher, A32733), Goat anti-Mouse IgG1 Cross-Adsorbed Secondary Antibody, Alexa Fluor 488 (1:1000; Thermofisher, A21121), Goat anti-Mouse IgG2a Cross-Adsorbed Secondary Antibody, Alexa Fluor 568 (1:1000; Thermofisher, A21134), Streptavidin, Alexa Fluor 546 conjugate (1:1000; Thermofisher, S11225), Donkey Anti-Goat IgG H&L (Alexa Fluor® 405) preadsorbed (1:1000; Abcam, ab175665), Donkey Anti-Rabbit IgG (H+L) Cross-adsorbed, Alexa Fluor 647 (1:1000; Thermofisher, A31573), Donkey Anti-Mouse IgG (H+L) Highly Cross-Adsorbed, Alexa Fluor 488 (1:1000; Thermofisher, A21202).

Additional methods can be found in the supplementary files.

575 ## Figure legends
576

577 **Figure 1: *Six2*^{GCiP} driven *Wt1*-mutant model characterization.**

578 (A) Schematic representation of the *Six2*^{GCiP} lineage specific knockout of *Wt1* in the mouse
579 model.
580 (B) *Ex vivo* kidney organ culture of E12.5 control (left) and *Wt1* mutant kidney (right), with
581 eGFP linked to SIX2 expression and TdTomato representing the lineage. Scale 200µm.
582 (C) Staining for SIX2, TdTomato and CDH1 on *ex vivo* kidney organ cultures of a control and
583 *Wt1* mutant kidney. Scale 100µm.
584 (D) H&E staining of control and *Wt1* mutant kidneys at E12.5. Scale 50µm.
585 (E) Staining for TdTomato to validate lineage and WT1 to validate knockout in E12.5 control
586 and mutant kidneys. Scale 100µm.
587 (F) H&E staining of control and *Wt1* mutant kidneys at E18.5. Scale 50µm.
588 (G) Staining for SIX2, CDH1 and WT1 to elucidate identity of E18.5 mutant kidneys. Scale
589 100µm.

590

591 **Figure 2: *Foxd1*^{GC} driven *Wt1*-mutant model characterization**

592 (A) Schematic representation of the *Foxd1*^{GC} lineage specific knockout of *Wt1* in the mouse
593 model.
594 (B) *Ex vivo* kidney organ culture of E12.5 control (left) and *Wt1* mutant kidney (right), with
595 eGFP linked to FOXD1 expression and TdTomato representing the lineage. Scale 200µm.
596 (C) Absolute quantification of the number of cap mesenchymes in the control versus mutant
597 kidney, quantified from the *ex vivo* kidney organ culture.
598 (D) Staining of DAPI and CDH1 on the *ex vivo* kidney culture. Scale 100µm.
599 (E) H&E staining of control and *Wt1* mutant kidneys at E12.5. Scale 50µm.

600 (F) Staining for TdTomato to validate lineage and WT1 to validate knockout in E12.5 control
601 and mutant kidneys. Scale 100μm. White arrowheads indicate Foxd1 lineage
602 contribution to SIX2+ cells.
603 (G) H&E staining of control and *Wt1* mutant kidneys at E18.5. Scale 50μm.
604 (H) Staining for TdTomato to validate lineage and WT1 to validate knockout in E18.5 control
605 and mutant kidneys. Scale 100μm. White open arrows indicate Foxd1-lineage in or
606 around proximal tubules.

607

608 **Figure 3: *Wt1^{CE}* driven *Wt1*-mutant model characterization**

609 (A) Schematic representation of the *Wt1^{CE}* spatial and temporal specific knockout of *Wt1* in
610 the mouse model.
611 (B) Optimization of Tx injection at E8.5, E9.5, E10.5 or E11.5, and double injections at E9.5 +
612 E10.5, analyzed in *ex vivo* kidney cultures at E12. Cells labeled with white arrows are a
613 representation of the tamoxifen treatment escaping cells. White arrowheads indicate
614 cap mesenchyme cells that escaped tamoxifen-induced Cre activation. Scale 60μm.
615 (C) *Ex vivo* kidney organ culture of E12.5 control (upper) and *Wt1* mutant kidney (lower), with
616 TdTomato representing the lineage. White arrows highlight epithelializing structures.
617 White arrowheads indicate epithelialized structures based on morphology of the cells.
618 Scale 200μm.
619 (D) H&E staining of control and *Wt1* mutant kidneys at E12.5. Scale 50μm.
620 (E) Staining for TdTomato to validate lineage and WT1 to validate knockout in E12.5 control
621 and mutant kidneys. White arrowheads indicate cap mesenchyme cells that escaped
622 tamoxifen-induced Cre activation. Scale 100μm.
623 (F) H&E staining of control and *Wt1* mutant kidneys at E18.5. Scale 50μm.

624 (G) Staining for TdTomato to validate lineage and WT1 to validate knockout in E18.5 control
625 and mutant kidneys. LTL marks proximal tubules. White arrows indicate nephrogenic(-
626 derived) WT1 expression indicating the escaped regions. Scale 100µm.

627

628 **Figure 4: Cancer Stem Cell marker expression in lineage-specific *Wt1* mutant kidneys**

629 (A) Staining for CSC markers NCAM1, ALDH1A2, SIX2 and CITED1 in the normal developing
630 embryonic kidney at E12.5 and E18.5. White arrows indicate triple-marker expressing
631 cells. Scale 100µm.
632 (B) CSC marker expression in *Six2*^{GCiP} driven *Wt1* mutant kidneys at E12.5 and E18.5. Scale
633 100µm.
634 (C) CSC marker expression in *Foxd1*^{GC} driven *Wt1* mutant kidneys at E12.5 and E18.5. White
635 arrows indicate triple-marker expressing cells. Scale 100µm.
636 (D) CSC marker expression in *Wt1*^{CE} driven *Wt1* mutant kidneys at E12.5 and E18.5. White
637 arrows indicate triple-marker expressing cells. Scale 100µm.

638

639 **Figure 5: Characterization of the LIN28B overexpression model**

640 (A) Schematic representation of the doxycycline inducible LIN28B overexpression model,
641 with (representing mutants) and without (representing doxycycline exposed control
642 littermates) tdTomato reporter.
643 (B) *Ex vivo* kidney organ culture of E12.5 control (upper) and LIN28B mutant kidney (lower).
644 Scale 200µm.
645 (C) H&E staining of control and LIN28B mutant kidneys at E12.5 (left panel) and E18.5 (right
646 panel). Scale 50µm.
647 (D) Staining for WT1, SIX2 and CDH1 to identify phenotype at E12.5 and E18.5. Scale 100µm.

648 (E) H&E staining of control and LIN28B mutant kidneys at P19. Scale 50µm.

649 (F) Staining for WT1, SIX2 and CDH1 to identify blastemal phenotype at P19. White arrows
650 indicate SIX2+WT1+ cells, orange arrows indicate SIX2-WT1+ cells, hinting towards
651 commitment to the epithelial lineage. Scale 100µm.

652

653 **Figure 6: Cancer Stem Cell marker expression in LIN28B overexpression mutant kidneys**

654 (A) CSC marker expression in E12.5 LIN28B overexpression kidneys. White arrows indicate
655 triple-marker expressing cells. Scale 100µm.

656 (B) CSC marker expression in E18.5 LIN28B overexpression kidneys, showing early
657 blastemal-like cells co-expressing all four markers in the same cells indicated by the
658 white arrows on consecutive sections. Scale 100µm.

659 (C) CSC marker expression in P19 LIN28B overexpression kidneys, showing blastemal-like
660 cells with distinct patterns for ALDH1A2 and CITED1 expression, and a transitional cell
661 co-expressing all four markers in the same cell. High protein expression is indicated with
662 an orange arrow, low protein expression with a green arrow and the transitional cells are
663 indicated with asterisks. Scale 100µm.

664

665 **Figure 7: Schematic representation of genotype-phenotype speculations of Wilms tumor**
666 **driver mutations.**

667 (A) CSC marker expression over the course of nephrogenesis, in the nephrogenic and
668 stromal lineage.

669 (B) *Six2*^{GCiP} driven loss of Wt1 results in severe block of nephrogenesis, and possibly results
670 in lineage confusion based on CSC marker expression.

671 (C) *Foxd1*^{GC} driven Wt1 loss results in expanded stroma and a ureteric bud branching
672 phenotype.
673 (D) Conditional loss of Wt1 through the *Wt1*^{CE} tamoxifen dependent administration results in
674 stromal and ureteric bud phenotype and a mild block of nephrogenesis. Here the first
675 suggestive quadruple-positive CSC markers come together in the same cells possibly
676 giving rise to blastema.
677 (E) LIN28B overexpression results in delayed nephron epithelialization, embryonic lobe
678 formation and blastemal-like cells co-expressing the four CSC markers.
679

680 # Supplementary

681

682 ## Supplementary methods

683 ### *Ncam1/ALDERED assay for flow cytometry*

684 Embryonic kidneys from E12.5 embryos were directly dissociated with Trypsin/EDTA (0.05%)
685 (Gibco, REF25300) for 3' at 37°C. (Embryonic) kidneys from E18.5 and P19 were first minced into
686 small pieces using a scalpel, prior to dissociation. After incubation, tissues were vigorously
687 pipetted up and down to dissociate into single cells. DMEM + 10% FCS was used to inactivate the
688 trypsin. Cells were centrifuged 5' at 300g and resuspended in FACS buffer (PBS + 0.5% BSA +
689 0.04M EDTA). Clumps were removed by using a 35µm cell strainer. A small fraction was taken at
690 this step to calibrate the flow cytometer. The rest of the single cells were stained for Ncam1
691 (1:125; NCAM-1/CD56 Antibody, R&D systems, AF2408) with a Donkey-anti-Goat Alexa Fluor 405
692 (1:1500; Abcam, ab175665), followed by the ALDERED assay kit (EMD Millipore, SCR150)
693 according to the manufacturer's protocol. LSRFortessa flow cytometer (BD Biosciences) was
694 used to measure expression.

695

696 ### *Statistical analysis*

697 Due to variable cytometer settings over time, raw data was normalized to paired littermate
698 controls. The DEAB sample was used as the threshold for ALDERED expression. Normalized
699 expression values were compared between controls and mutants from the same time point and
700 Cre driver. Wt1-mutants: Six2-Cre driven E12.5 ctrl (n=9) vs mutant (n=7), Six2-Cre driven E18.5
701 ctrl (n=10) vs mutant (n=6), Foxd1-Cre driven E12.5 ctrl (n=13) vs mutant (n=4), Foxd1-Cre driven
702 E18.5 ctrl (n=14) vs mutant (n=5), Wt1-CE driven E12.5 ctrl (n=9) vs mutant (n=8), Wt1-CE driven
703 E18.5 ctrl (n=6) vs mutant (n=6)). LIN28B mutants: E12.5 ctrl (n=6) vs mutant (n=6) and E18.5 ctrl

704 (n=6) vs mutant (n=6). Groups were compared using a non-parametric Mann-Whitney U test
705 between groups.
706

707 ## Supplementary Figure legends

708 **Sup. Fig. 1: *Foxd1^{GC}* driven *Wt1* mutant.** SIX2+ caps lost their apical orientation and started
709 moving inwards. Scale 100µm.

710

711 **Sup. Fig. 2: NCAM1+/ALDERED flowcytometry assay on Wt1 mutant embryonic kidneys.**

712 (A) Fraction of NCAM1+/ALDERED double positive cells in developing embryonic kidneys
713 comparing control versus Wt1 mutants from the three lineage-specific Cre-drivers at
714 E12.5 and E18.5. No significant differences observed between groups, using a non-
715 parametric Mann-Whitney U test between groups. P-values indicated.
716 (B) Raw data files from the *Six2^{GCiP}* driven control versus mutant kidneys, using DEAB for
717 setting the cutoff for the ALDH activity measured through ALDERED expression.
718 (C) Raw data files from the *Foxd1^{GC}* driven control versus mutant kidneys, using DEAB for
719 setting the cutoff for the ALDH activity measured through ALDERED expression.
720 (D) Raw data files from the *Wt1^{CE}* driven control versus mutant kidneys, using DEAB for
721 setting the cutoff for the ALDH activity measured through ALDERED expression.

722

723 **Sup. Fig. 3: ALDH paralogue expression in Wilms tumor Xenograft microarray data and in**
724 **developing kidneys**

725 (A) ALDH paralogue enrichment in Wilms tumor Xenograft derived CSCs. A comparison
726 between unsorted and sorted fractions, for NCAM1+/ALDEFLUOR- and
727 NCAM1+/ALDEFLUOR+.

728 (B) ALDH paralogue protein staining in *ex vivo* kidney cultures, cultured for 24, 48 and 72
729 hours. Scale bar: 50µm.
730 (C) FOXD1 and ALDH1A2 protein expression in ex vivo kidney cultures cultured for 96 hours.
731 Scale bar: 50µm.

732

733 **Sup. Fig. 4: NCAM1+/ALDERED flowcytometry assay on LIN28B mutant embryonic kidneys.**

734 (A) Fraction of NCAM1+/ALDERED double positive cells in developing embryonic kidneys
735 comparing control versus LIN28B mutants at E12.5 and E18.5. No significant differences
736 observed between groups, using a non-parametric Mann-Whitney U test between
737 groups.
738 (B) Raw data files from the control versus mutant kidneys at E12.5, using DEAB for setting
739 the cutoff for the ALDH activity measured through ALDERED expression.
740 (C) Raw data files from the control versus mutant kidneys at E18.5, using DEAB for setting
741 the cutoff for the ALDH activity measured through ALDERED expression.

742

743 **Sup. Fig. 5: Proliferative marker expression KI67 in *Wt1* and LIN28B mutant (developing)**
744 **kidneys.**

745 (A) KI67 staining for Wt1 mutant kidneys at E12.5 for lineage-specific Cre drivers. Scale
746 100µm.
747 (B) KI67 staining for Wt1 mutant kidneys at E18.5 for lineage-specific Cre drivers. Scale
748 100µm.
749 (C) KI67 staining for LIN28B mutant kidneys at P19. Scale 100µm.

750

Author contributions

N.S.P. performed and analyzed all experiments. D.K., C.M.B, M.M.L., J.W.C.C., C.W.J.C and D.D.Ö supported in the performed experiments and contributed to the supplementary figures. N.S.P and P.H. designed the experiments. N.S.P. prepared figures. N.S.P., K.S.D. and P.H. wrote the manuscript.

Acknowledgements

We thank all members of the Hohenstein lab for valuable discussions. We thank Jorrit Hos and Orhan Demirbacak for help with animals. The research was supported by KiKa (Children Cancer Free Foundation).

Conflict of interest

The authors declare no competing interests.

References

Armstrong, J. F., Pritchard-Jones, K., Bickmore, W. A., Hastie, N. D. and Bard, J. B. (1993). The expression of the Wilms' tumour gene, WT1, in the developing mammalian embryo. *Mech Dev* **40**, 85-97.

Beckwith, J. B., Kiviat, N. B. and Bonadio, J. F. (1990). Nephrogenic rests, nephroblastomatosis, and the pathogenesis of Wilms' tumor. *Pediatr Pathol* **10**, 1-36.

Berry, R. L., Ozdemir, D. D., Aronow, B., Lindstrom, N. O., Dudnakova, T., Thornburn, A., Perry, P., Baldock, R., Armit, C., Joshi, A. et al. (2015). Deducing the stage of origin of Wilms' tumours from a developmental series of Wt1-mutant mice. *Dis Model Mech* **8**, 903-17.

Bonnet, D. and Dick, J. E. (1997). Human acute myeloid leukemia is organized as a hierarchy that originates from a primitive hematopoietic cell. *Nat Med* **3**, 730-7.

Cotino-Najera, S., Garcia-Villa, E., Cruz-Rosales, S., Gariglio, P. and Diaz-Chavez, J. (2024). The role of Lin28A and Lin28B in cancer beyond Let-7. *FEBS Lett* **598**, 2963-2979.

Davies, J. A., Ladomery, M., Hohenstein, P., Michael, L., Shafe, A., Spraggon, L. and Hastie, N. (2004). Development of an siRNA-based method for repressing specific genes in renal organ culture and its use to show that the Wt1 tumour suppressor is required for nephron differentiation. *Hum Mol Genet* **13**, 235-46.

Dolt, K. S., Lawrence, M. L., Miller-Hodges, E., Slight, J., Thornburn, A., Devenney, P. S. and Hohenstein, P. (2013). A universal vector for high-efficiency multi-fragment recombineering of BACs and knock-in constructs. *PLoS One* **8**, e62054.

Essafi, A., Webb, A., Berry, R. L., Slight, J., Burn, S. F., Spraggon, L., Velecela, V., Martinez-Estrada, O. M., Wiltshire, J. H., Roberts, S. G. et al. (2011). A Wt1-controlled chromatin switching mechanism underpins tissue-specific Wnt4 activation and repression. *Dev Cell* **21**, 559-74.

Ginestier, C., Hur, M. H., Charafe-Jauffret, E., Monville, F., Dutcher, J., Brown, M., Jacquemier, J., Viens, P., Kleer, C. G., Liu, S. et al. (2007). ALDH1 is a marker of normal and malignant human mammary stem cells and a predictor of poor clinical outcome. *Cell Stem Cell* **1**, 555-67.

Hohenstein, P. and Hastie, N. D. (2006). The many facets of the Wilms' tumour gene, WT1. *Hum Mol Genet* **15 Spec No 2**, R196-201.

Hohenstein, P., Pritchard-Jones, K. and Charlton, J. (2015). The yin and yang of kidney development and Wilms' tumors. *Genes Dev* **29**, 467-82.

Kobayashi, A., Mugford, J. W., Krautzberger, A. M., Naiman, N., Liao, J. and McMahon, A. P. (2014). Identification of a Multipotent Self-Renewing Stromal Progenitor Population during Mammalian Kidney Organogenesis. *Stem Cell Reports* **3**, 650-62.

Kobayashi, A., Valerius, M. T., Mugford, J. W., Carroll, T. J., Self, M., Oliver, G. and McMahon, A. P. (2008). Six2 defines and regulates a multipotent self-renewing nephron progenitor population throughout mammalian kidney development. *Cell Stem Cell* **3**, 169-81.

Kreidberg, J. A., Sariola, H., Loring, J. M., Maeda, M., Pelletier, J., Housman, D. and Jaenisch, R. (1993). WT-1 is required for early kidney development. *Cell* **74**, 679-691.

Li, M., Chen, H. and Wu, T. (2019). LIN28: A cancer stem cell promoter for immunotherapy in head and neck squamous cell carcinoma. *Oral Oncol* **98**, 92-95.

Li, Y., Gong, H., Ding, J., Zhao, F., Du, J., Wan, J., Zhang, J., Liu, S., Li, J., Wang, L. et al. (2020). Inhibition of GSK3 Represses the Expression of Retinoic Acid Synthetic Enzyme ALDH1A2 via Wnt/β-Catenin Signaling in WiT49 Cells. *Frontiers in Cell and Developmental Biology* **8**.

Li, Y., Wang, L., Ai, W., He, N., Zhang, L., Du, J., Wang, Y., Mao, X., Ren, J., Xu, D. et al. (2017). Regulation of retinoic acid synthetic enzymes by WT1 and HDAC inhibitors in 293 cells. *Int J Mol Med* **40**, 661-672.

Lindstrom, N. O., McMahon, J. A., Guo, J., Tran, T., Guo, Q., Rutledge, E., Parvez, R. K., Saribekyan, G., Schuler, R. E., Liao, C. et al. (2018). Conserved and Divergent Features of Human and Mouse Kidney Organogenesis. *J Am Soc Nephrol* **29**, 785-805.

Madisen, L., Garner, A. R., Shimaoka, D., Chuong, A. S., Klapoetke, N. C., Li, L., van der Bourg, A., Niino, Y., Egolf, L., Monetti, C. et al. (2015). Transgenic mice for intersectional targeting of neural sensors and effectors with high specificity and performance. *Neuron* **85**, 942-58.

Madisen, L., Zwingman, T. A., Sunkin, S. M., Oh, S. W., Zariwala, H. A., Gu, H., Ng, L. L., Palmiter, R. D., Hawrylycz, M. J., Jones, A. R. et al. (2010). A robust and high-throughput Cre reporting and characterization system for the whole mouse brain. *Nat Neurosci* **13**, 133-40.

Markovic-Lipkovski, J., Muller, C. A., Klein, G., Flad, T., Klatt, T., Blaschke, S., Wessels, J. T. and Muller, G. A. (2007). Neural cell adhesion molecule expression on renal interstitial cells. *Nephrol Dial Transplant* **22**, 1558-66.

Martinez-Estrada, O. M., Lettice, L. A., Essafi, A., Guadix, J. A., Slight, J., Velecela, V., Hall, E., Reichmann, J., Devenney, P. S., Hohenstein, P. et al. (2010). Wt1 is required for cardiovascular progenitor cell formation through transcriptional control of Snail and E-cadherin. *Nat Genet* **42**, 89-93.

McMahon, A. P. (2016). Development of the Mammalian Kidney. *Curr Top Dev Biol* **117**, 31-64.

Miyagawa, K., Kent, J., Moore, A., Charlieu, J. P., Little, M. H., Williamson, K. A., Kelsey, A., Brown, K. W., Hassam, S., Briner, J. et al. (1998). Loss of WT1 function leads to ectopic myogenesis in Wilms' tumour. *Nat Genet* **18**, 15-7.

Mugford, J. W., Yu, J., Kobayashi, A. and McMahon, A. P. (2009). High-resolution gene expression analysis of the developing mouse kidney defines novel cellular compartments within the nephron progenitor population. *Dev Biol* **333**, 312-23.

Murphy, A. J., Pierce, J., de Caestecker, C., Taylor, C., Anderson, J. R., Perantoni, A. O., de Caestecker, M. P. and Lovvorn, H. N., 3rd. (2012). SIX2 and CITED1, markers of nephronic progenitor self-renewal, remain active in primitive elements of Wilms' tumor. *J Pediatr Surg* **47**, 1239-49.

Naiman, N., Fujioka, K., Fujino, M., Valerius, M. T., Potter, S. S., McMahon, A. P. and Kobayashi, A. (2017). Repression of Interstitial Identity in Nephron Progenitor Cells by Pax2 Establishes the Nephron-Interstitium Boundary during Kidney Development. *Dev Cell* **41**, 349-365 e3.

Niculovic, K. M., Vicente, M. M., Wittek, V., Kats, E., Albers, I., Flachsig-Schulz, K., Peters-Bernard, U., Weiss, A. C., Thiesler, H., Drager, L. S. et al. (2025). Polysialic acid regulates glomerular microvasculature formation by interaction with VEGF-A188 in mice. *Angiogenesis* **28**, 31.

Niederreither, K., Subbarayan, V., Dollé, P. and Chambon, P. (1999). Embryonic retinoic acid synthesis is essential for early mouse post-implantation development. *Nature Genetics* **21**, 444-448.

O'Brien, L. L., Guo, Q., Bahrami-Samani, E., Park, J. S., Hasso, S. M., Lee, Y. J., Fang, A., Kim, A. D., Guo, J., Hong, T. M. et al. (2018). Transcriptional regulatory control of mammalian nephron progenitors revealed by multi-factor cistromic analysis and genetic studies. *PLoS Genet* **14**, e1007181.

Petrosyan, A., Villani, V., Aguiari, P., Thornton, M. E., Wang, Y., Rajewski, A., Zhou, S., Cravedi, P., Grubbs, B. H., De Filippo, R. E. et al. (2023). Identification and Characterization of the Wilms Tumor Cancer Stem Cell. *Adv Sci (Weinh)*, e2206787.

Pode-Shakked, N., Metsuyanim, S., Rom-Gross, E., Mor, Y., Fridman, E., Goldstein, I., Amariglio, N., Rechavi, G., Keshet, G. and Dekel, B. (2009). Developmental tumourigenesis: NCAM as a putative marker for the malignant renal stem/progenitor cell population. *J Cell Mol Med* **13**, 1792-808.

Pode-Shakked, N., Shukrun, R., Mark-Danieli, M., Tsvetkov, P., Bahar, S., Pri-Chen, S., Goldstein, R. S., Rom-Gross, E., Mor, Y., Fridman, E. et al. (2013). The isolation and characterization of renal cancer initiating cells from human Wilms' tumour xenografts unveils new therapeutic targets. *EMBO Mol Med* **5**, 18-37.

Schumacher, V., Schuhen, S., Sonner, S., Weirich, A., Leuschner, I., Harms, D., Licht, J., Roberts, S. and Royer-Pokora, B. (2003). Two molecular subgroups of Wilms' tumors with or without WT1 mutations. *Clin Cancer Res* **9**, 2005-14.

863 **Shukrun, R., Pode-Shakked, N., Pleniceanu, O., Omer, D., Vax, E., Peer, E., Pri-Chen, S.,**
864 **Jacob, J., Hu, Q., Harari-Steinberg, O. et al.** (2014). Wilms' tumor blastemal stem cells
865 dedifferentiate to propagate the tumor bulk. *Stem Cell Reports* **3**, 24-33.
866 **Spreafico, F., Fernandez, C. V., Brok, J., Nakata, K., Vujanic, G., Geller, J. I., Gessler, M.,**
867 **Maschietto, M., Behjati, S., Polanco, A. et al.** (2021). Wilms tumour. *Nat Rev Dis Primers* **7**, 75.
868 **Urbach, A., Yermalovich, A., Zhang, J., Spina, C. S., Zhu, H., Perez-Atayde, A. R., Shukrun,**
869 **R., Charlton, J., Sebire, N., Mifsud, W. et al.** (2014). Lin28 sustains early renal progenitors and
870 induces Wilms tumor. *Genes Dev* **28**, 971-82.
871 **Viswanathan, S. R. and Daley, G. Q.** (2010). Lin28: A microRNA regulator with a macro role.
872 *Cell* **140**, 445-9.
873 **Wegert, J., Zauter, L., Appenzeller, S., Otto, C., Bausenwein, S., Vokuhl, C., Ernestus, K.,**
874 **Furtwangler, R., Graf, N. and Gessler, M.** (2020). High-risk blastemal Wilms tumor can be modeled
875 by 3D spheroid cultures in vitro. *Oncogene* **39**, 849-861.
876 **Weiss, A. C., Rivera-Reyes, R., Englert, C. and Kispert, A.** (2020). Expansion of the renal
877 capsular stroma, ureteric bud branching defects and cryptorchidism in mice with Wilms tumor 1
878 gene deletion in the stromal compartment of the developing kidney. *J Pathol* **252**, 290-303.
879 **Yermalovich, A. V., Osborne, J. K., Sousa, P., Han, A., Kinney, M. A., Chen, M. J., Robinton,**
880 **D. A., Montie, H., Pearson, D. S., Wilson, S. B. et al.** (2019). Lin28 and let-7 regulate the timing of
881 cessation of murine nephrogenesis. *Nat Commun* **10**, 168.
882 **Zheng, H., Liu, J., Pan, X. and Cui, X.** (2023). Biomarkers for patients with Wilms tumor: a
883 review. *Front Oncol* **13**, 1137346.
884 **Zhou, B., Ma, Q., Rajagopal, S., Wu, S. M., Domian, I., Rivera-Feliciano, J., Jiang, D., von**
885 **Gise, A., Ikeda, S., Chien, K. R. et al.** (2008). Epicardial progenitors contribute to the cardiomyocyte
886 lineage in the developing heart. *Nature* **454**, 109-13.
887 **Zhou, J., Ng, S. B. and Chng, W. J.** (2013). LIN28/LIN28B: an emerging oncogenic driver in
888 cancer stem cells. *Int J Biochem Cell Biol* **45**, 973-8.
889 **Zhou, L., Sheng, D., Wang, D., Ma, W., Deng, Q., Deng, L. and Liu, S.** (2019). Identification of
890 cancer-type specific expression patterns for active aldehyde dehydrogenase (ALDH) isoforms in
891 ALDEFLUOR assay. *Cell Biol Toxicol* **35**, 161-177.

892

893

Figure1

A.

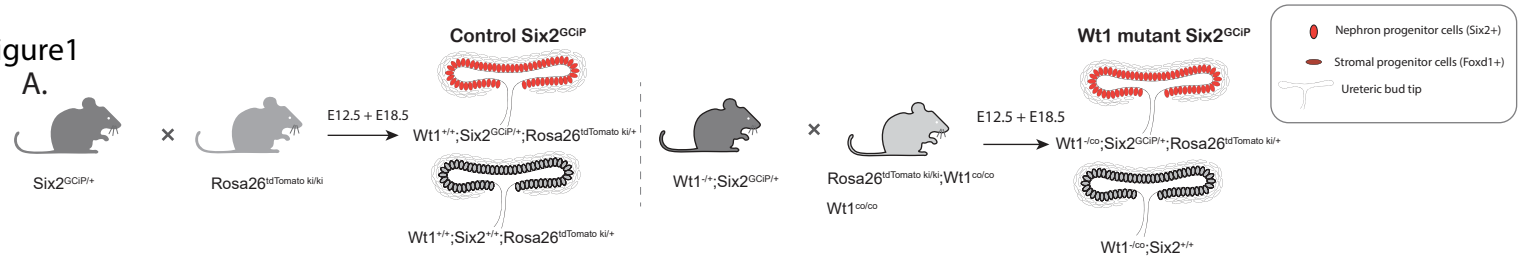

B.

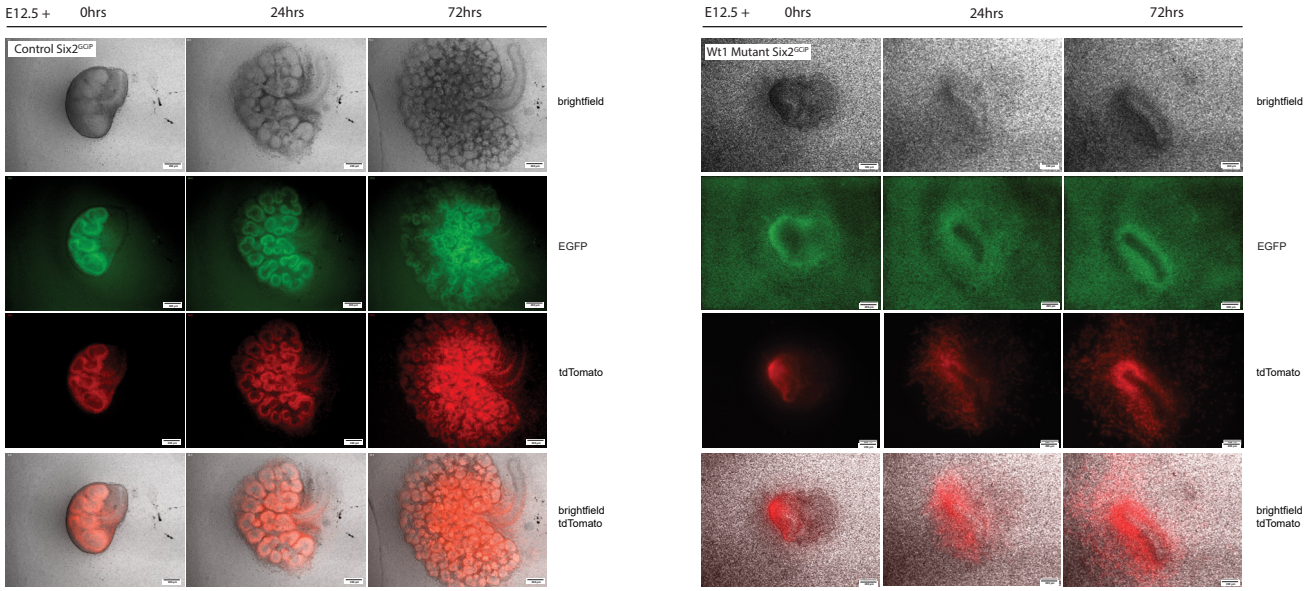

C.

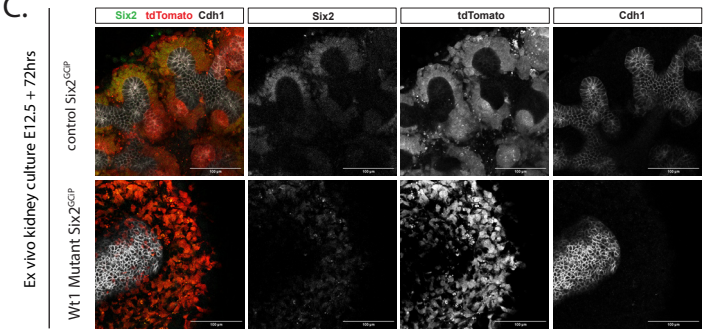

D.

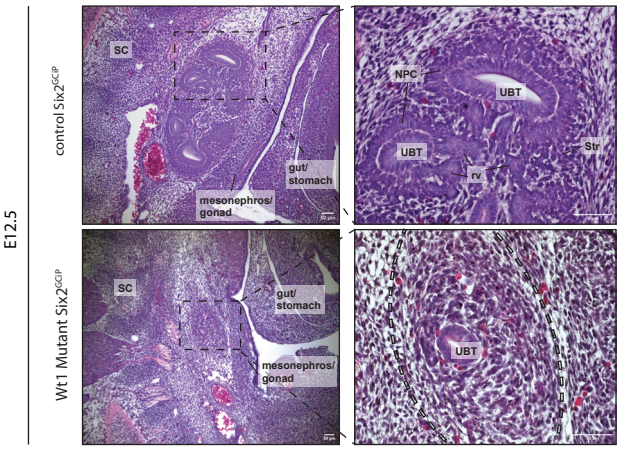

E.

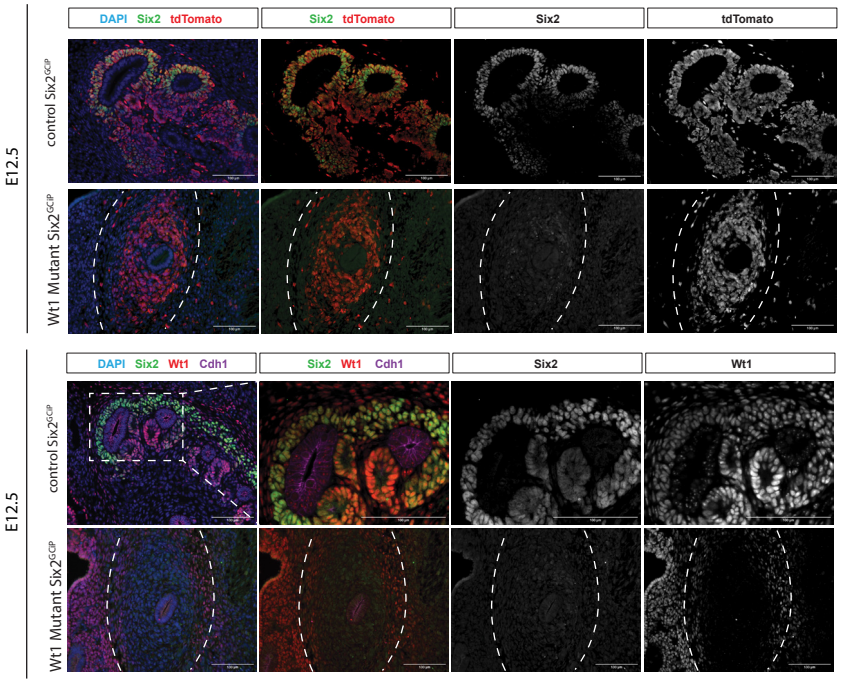

F.

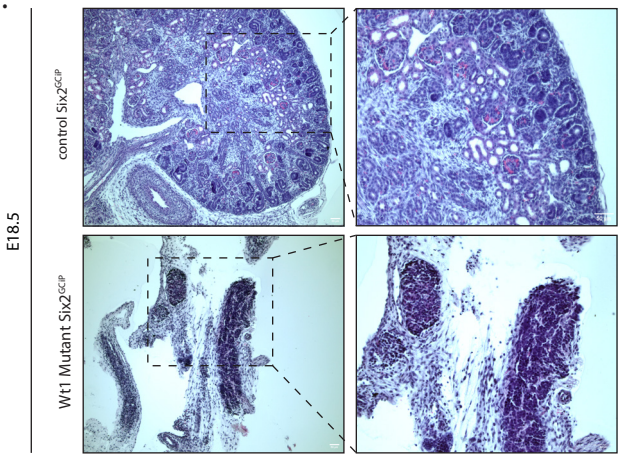

G.

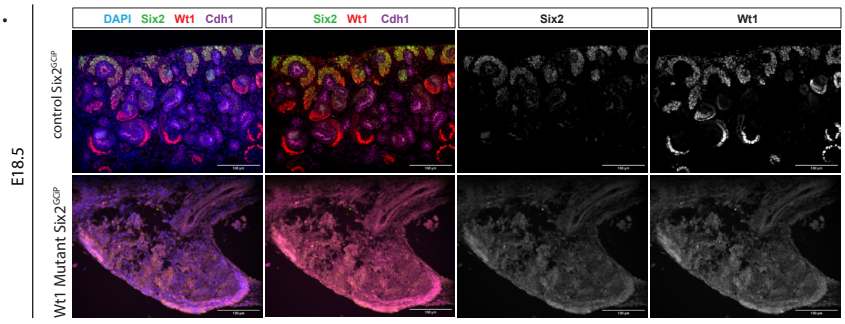

Figure 2

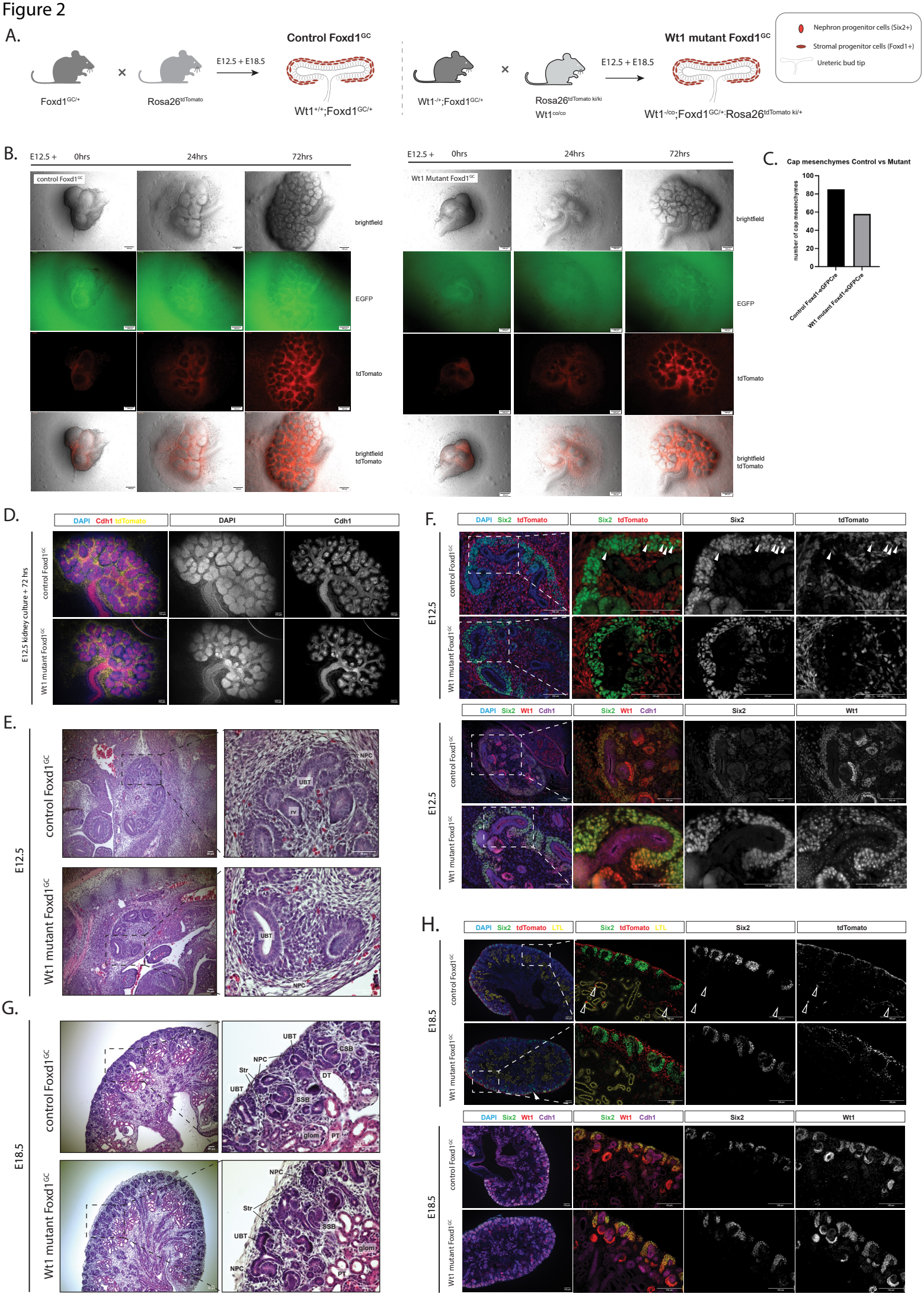
A.
Control Foxd1GC
Foxd1GC/+
Rosa26tdTomato
E12.5 + E18.5
Wt1+/+;Foxd1GC/+
Wt1 mutant Foxd1GC
Wt1-/+;Foxd1GC/+
Rosa26tdTomato ki/ki
Wt1co/co
Wt1-/co;Foxd1GC/+;Rosa26tdTomato ki/+
Nephron progenitor cells (Six2+)
Stromal progenitor cells (Foxd1+)
Ureteric bud tip
B.
E12.5 +
0hrs
24hrs
72hrs
control Foxd1GC
Wt1 Mutant Foxd1GC
brightfield
EGFP
tdTomato
brightfield tdTomato
C.
Cap mesenchymes Control vs Mutant
number of cap mesenchymes
100
80
60
40
20
0
Control Foxd1-eGFPCre
Wt1 mutant Foxd1-eGFPCre
D.
E12.5 kidney culture + 72 hrs
DAPI Cdh1 tdTomato
DAPI
Cdh1
control Foxd1GC
Wt1 mutant Foxd1GC
E.
E12.5
control Foxd1GC
Wt1 mutant Foxd1GC
NPC
UBT
rv
G.
E18.5
control Foxd1GC
Wt1 mutant Foxd1GC
UBT
NPC
Str
CSB
DT
SSB
glom
PT
F.
DAPI Six2 tdTomato
Six2 tdTomato
Six2
tdTomato
DAPI Six2 Wt1 Cdh1
Six2 Wt1 Cdh1
Wt1
H.
DAPI Six2 tdTomato LTL
Six2 tdTomato LTL

Figure 3

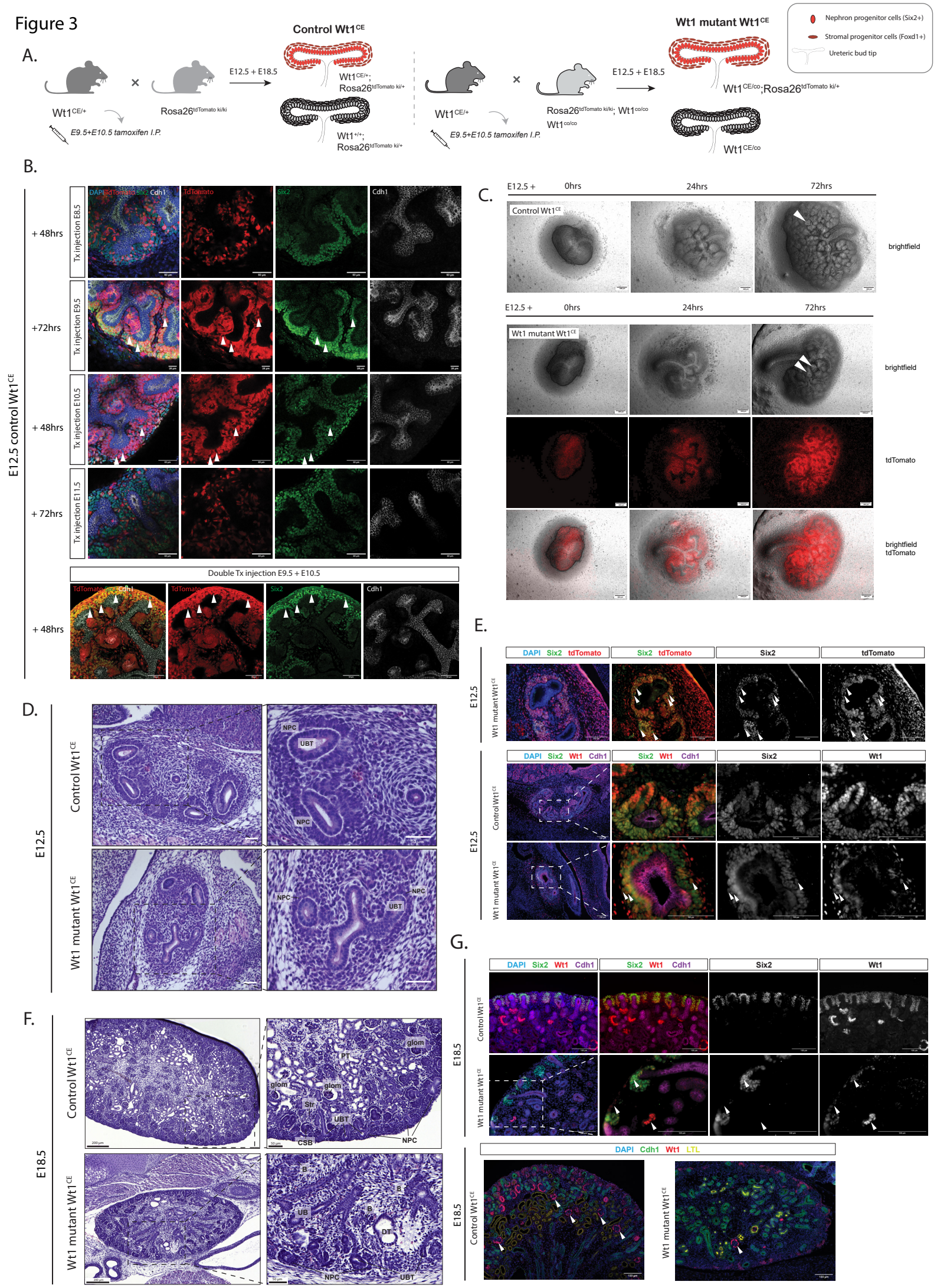
A.
Control Wt1CE
Wt1 mutant Wt1CE
Nephron progenitor cells (Six2+)
Stromal progenitor cells (Foxd1+)
Ureteric bud tip
Wt1CE/+
Rosa26tdTomato ki/ki
E9.5+E10.5 tamoxifen I.P.
E12.5 + E18.5
Wt1CE/+; Rosa26tdTomato ki/+
Wt1+/+; Rosa26tdTomato ki/+
Rosa26tdTomato ki/ki; Wt1co/co
Wt1co/co
Wt1CE/co;Rosa26tdTomato ki/+
Wt1CE/co
B.
E12.5 control Wt1CE
+ 48hrs
Tx injection E8.5
+72hrs
Tx injection E9.5
+ 48hrs
Tx injection E10.5
+ 72hrs
Tx injection E11.5
Double Tx injection E9.5 + E10.5
+ 48hrs
DAPI TdTomato Six2 Cdh1
TdTomato
Six2
Cdh1
C.
E12.5 +
0hrs
24hrs
72hrs
Control Wt1CE
Wt1 mutant Wt1CE
brightfield
tdTomato
brightfield tdTomato
D.
E12.5
Control Wt1CE
Wt1 mutant Wt1CE
NPC
UBT
E.
E12.5
DAPI Six2 tdTomato
Six2 tdTomato
Six2
tdTomato
DAPI Six2 Wt1 Cdh1
Six2 Wt1 Cdh1
Six2
Wt1
F.
E18.5
Control Wt1CE
Wt1 mutant Wt1CE
glom
PT
Str
UBT
CSB
NPC
B
UB
DT
G.
E18.5
DAPI Six2 Wt1 Cdh1
Six2 Wt1 Cdh1
Six2
Wt1
DAPI Cdh1 Wt1 LTL

Figure 4

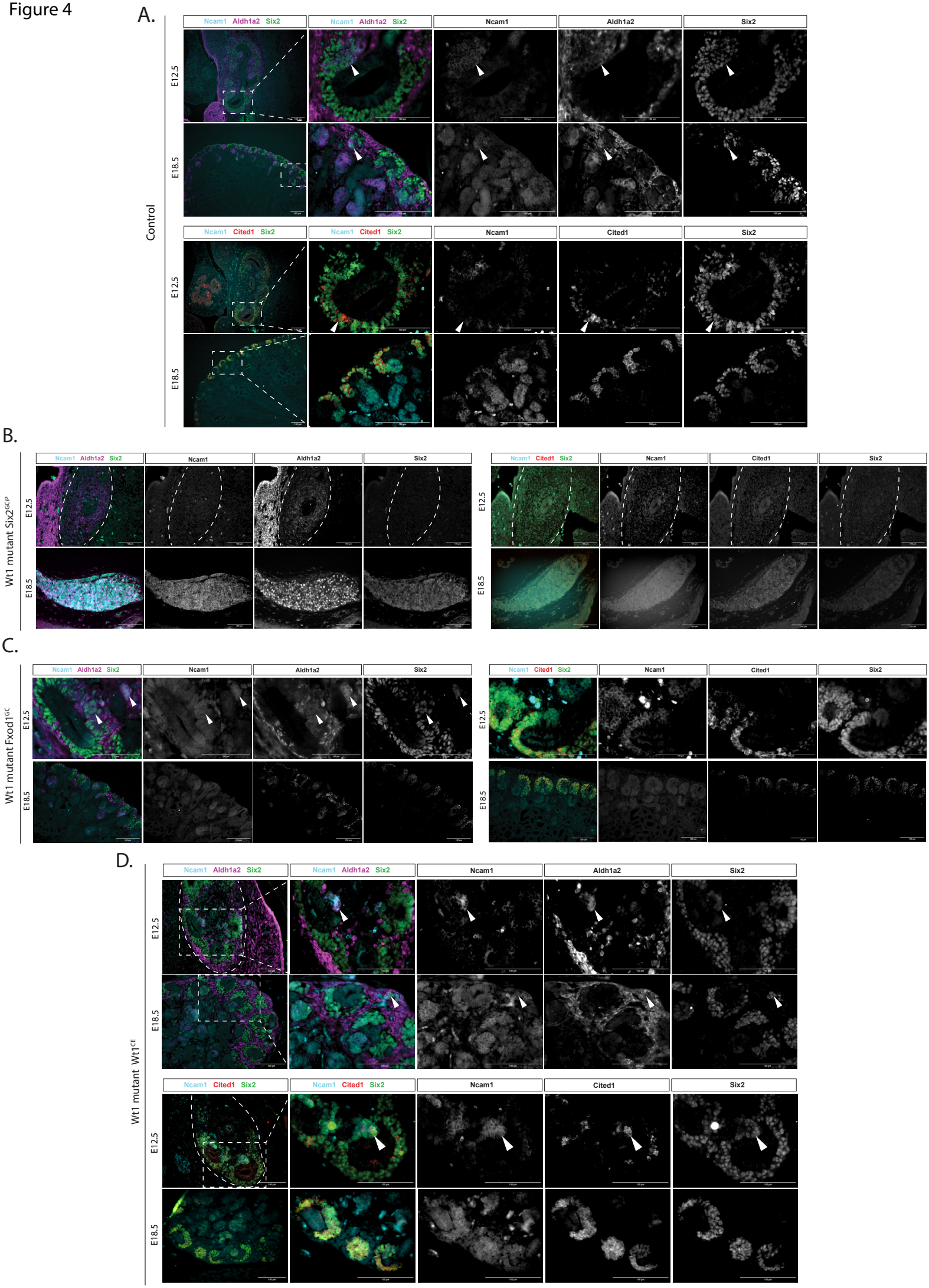
A.
Control
E12.5
E18.5
Ncam1 Aldh1a2 Six2
Ncam1 Aldh1a2 Six2
Ncam1
Aldh1a2
Six2
Ncam1 Cited1 Six2
Ncam1 Cited1 Six2
Ncam1
Cited1
Six2
B.
Wt1 mutant Six2GCIP
E12.5
E18.5
Ncam1 Aldh1a2 Six2
Ncam1
Aldh1a2
Six2
Ncam1 Cited1 Six2
Ncam1
Cited1
Six2
C.
Wt1 mutant Fxod1GC
E12.5
E18.5
Ncam1 Aldh1a2 Six2
Ncam1
Aldh1a2
Six2
Ncam1 Cited1 Six2
Ncam1
Cited1
Six2
D.
Wt1 mutant Wt1CE
E12.5
E18.5
Ncam1 Aldh1a2 Six2
Ncam1 Aldh1a2 Six2
Ncam1
Aldh1a2
Six2
Ncam1 Cited1 Six2
Ncam1 Cited1 Six2
Ncam1
Cited1
Six2

Figure 5

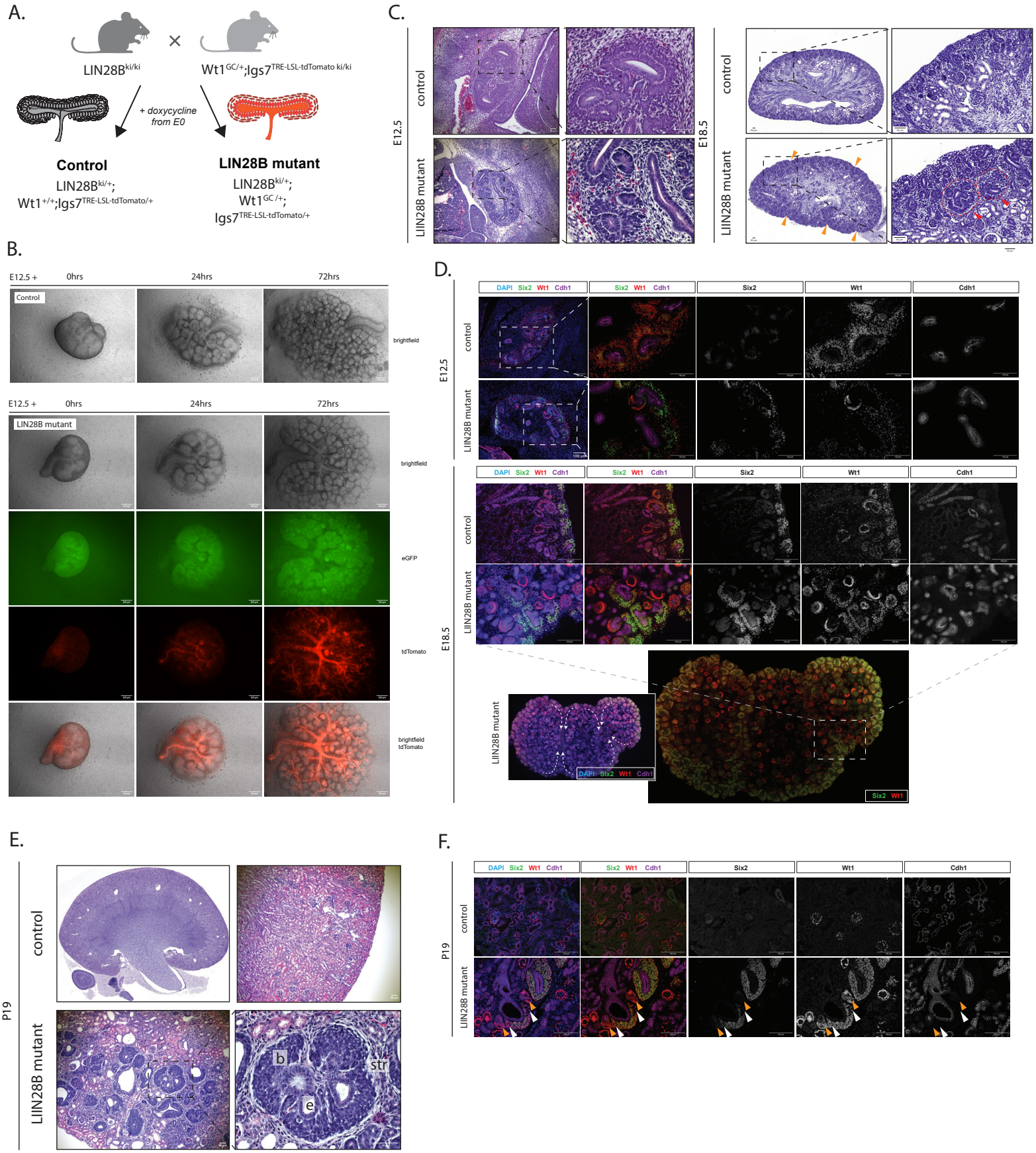
A.
LIN28B ki/ki
Wt1 GC/+;Igs7 TRE-LSL-tdTomato ki/ki
+ doxycycline from E0
Control
LIN28B ki/+; Wt1 +/+;Igs7 TRE-LSL-tdTomato/+
LIN28B mutant
LIN28B ki/+; Wt1 GC /+; Igs7 TRE-LSL-tdTomato/+
B.
E12.5 +
0hrs
24hrs
72hrs
Control
LIN28B mutant
brightfield
eGFP
tdTomato
brightfield tdTomato
C.
E12.5
E18.5
control
LIIN28B mutant
D.
DAPI Six2 Wt1 Cdh1
Six2 Wt1 Cdh1
Six2
Wt1
Cdh1
E.
P19
b
str
e
F.

Figure 6

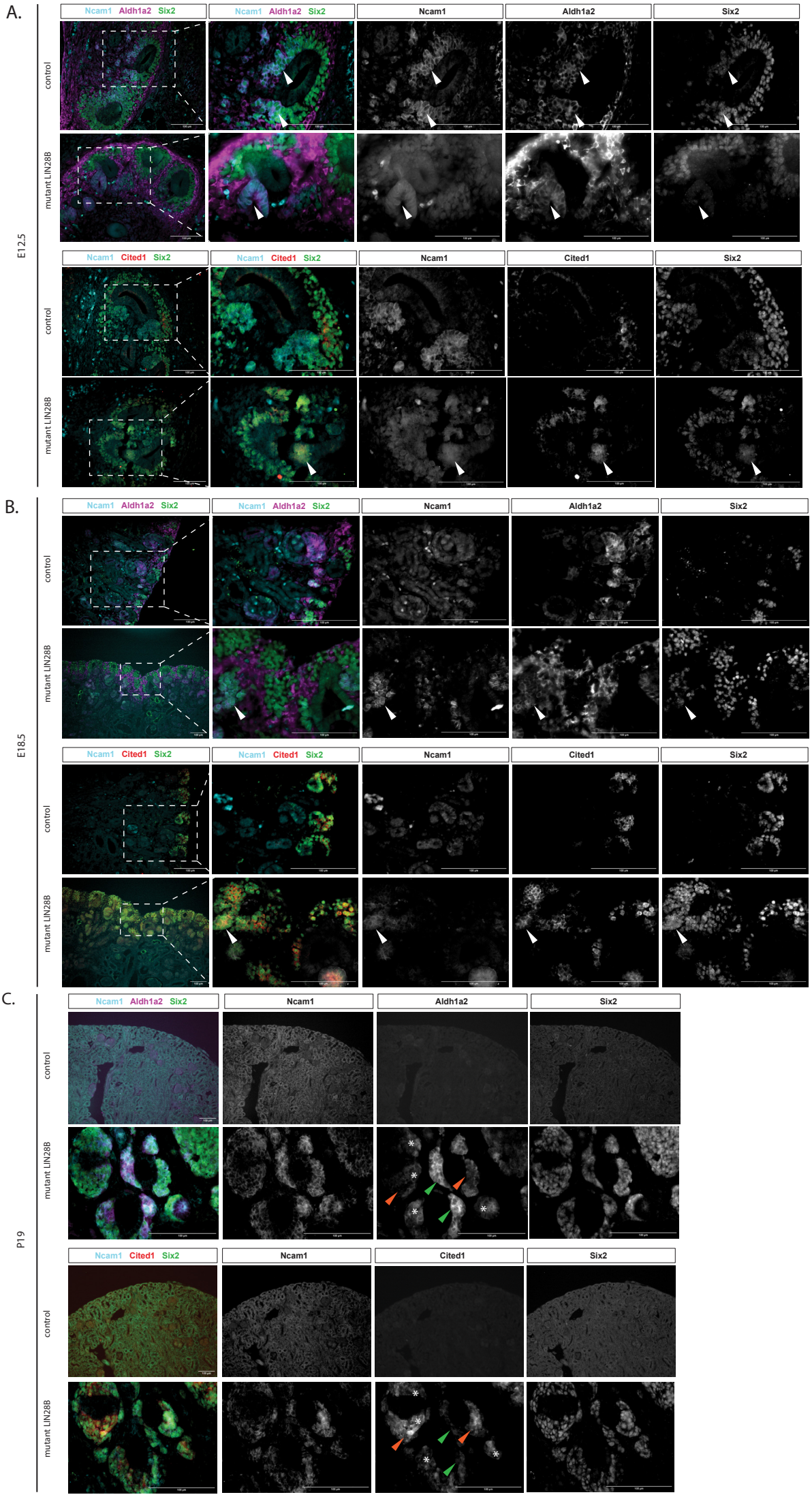
A.
E12.5
control
mutant LIN28B
Ncam1 Aldh1a2 Six2
Ncam1 Aldh1a2 Six2
Ncam1
Aldh1a2
Six2
Ncam1 Cited1 Six2
Ncam1 Cited1 Six2
Ncam1
Cited1
Six2
B.
E18.5
control
mutant LIN28B
Ncam1 Aldh1a2 Six2
Ncam1 Aldh1a2 Six2
Ncam1
Aldh1a2
Six2
Ncam1 Cited1 Six2
Ncam1 Cited1 Six2
Ncam1
Cited1
Six2
C.
P19
control
mutant LIN28B
Ncam1 Aldh1a2 Six2
Ncam1
Aldh1a2
Six2
Ncam1 Cited1 Six2
Ncam1
Cited1
Six2

Figure 7

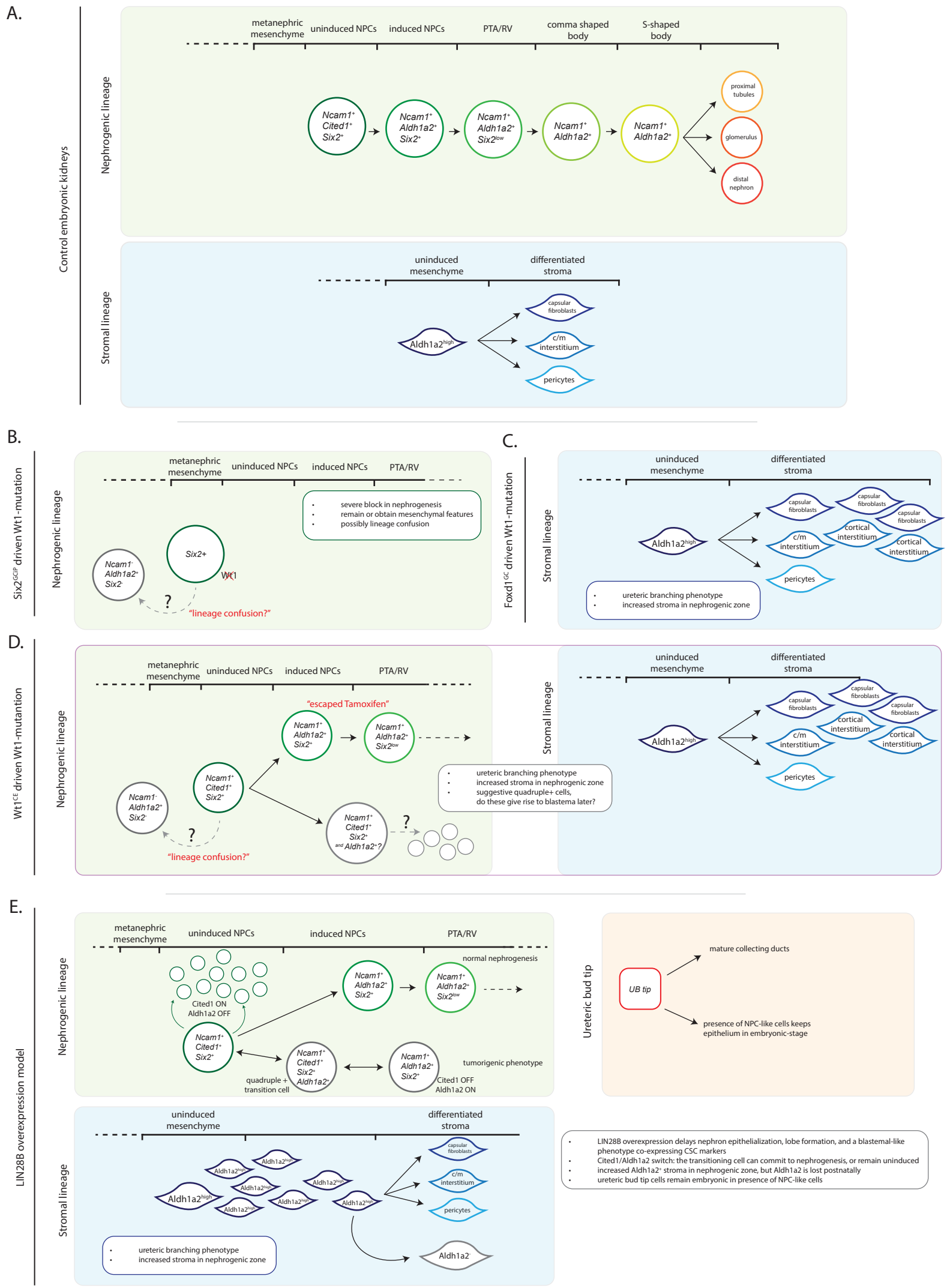
A.
Control embryonic kidneys
Nephrogenic lineage
metanephric mesenchyme
uninduced NPCs
induced NPCs
PTA/RV
comma shaped body
S-shaped body
Ncam1+ Cited1+ Six2+
Ncam1+ Aldh1a2+ Six2+
Ncam1+ Aldh1a2+ Six2low
Ncam1+ Aldh1a2+
Ncam1+ Aldh1a2+
proximal tubules
glomerulus
distal nephron
Stromal lineage
uninduced mesenchyme
differentiated stroma
Aldh1a2high
capsular fibroblasts
c/m interstitium
pericytes
B.
Six2GCIP driven Wt1-mutation
Nephrogenic lineage
metanephric mesenchyme
uninduced NPCs
induced NPCs
PTA/RV
severe block in nephrogenesis
remain or obtain mesenchymal features
possibly lineage confusion
Ncam1- Aldh1a2+ Six2-
Six2+
Wt1
"lineage confusion?"
C.
Foxd1GC driven Wt1-mutation
Stromal lineage
uninduced mesenchyme
differentiated stroma
Aldh1a2high
capsular fibroblasts
c/m interstitium
cortical interstitium
pericytes
ureteric branching phenotype
increased stroma in nephrogenic zone
D.
Wt1CE driven Wt1-mutantion
Nephrogenic lineage
metanephric mesenchyme
uninduced NPCs
induced NPCs
PTA/RV
"escaped Tamoxifen"
Ncam1+ Aldh1a2+ Six2+
Ncam1+ Aldh1a2+ Six2low
Ncam1+ Cited1+ Six2+
Ncam1- Aldh1a2+ Six2-
Ncam1+ Cited1+ Six2+ and Aldh1a2+?
"lineage confusion?"
ureteric branching phenotype
increased stroma in nephrogenic zone
suggestive quadruple+ cells, do these give rise to blastema later?
Stromal lineage
uninduced mesenchyme
differentiated stroma
Aldh1a2high
capsular fibroblasts
c/m interstitium
cortical interstitium
pericytes
E.
LIN28B overexpression model
Nephrogenic lineage
metanephric mesenchyme
uninduced NPCs
induced NPCs
PTA/RV
normal nephrogenesis
Cited1 ON Aldh1a2 OFF
Ncam1+ Cited1+ Six2+
Ncam1+ Aldh1a2+ Six2+
Ncam1+ Aldh1a2+ Six2low
Ncam1+ Cited1+ Six2+ Aldh1a2+
Ncam1+ Aldh1a2+ Six2+
tumorigenic phenotype
quadruple + transition cell
Cited1 OFF Aldh1a2 ON
Ureteric bud tip
UB tip
mature collecting ducts
presence of NPC-like cells keeps epithelium in embryonic-stage
Stromal lineage
uninduced mesenchyme
differentiated stroma
Aldh1a2high
Aldh1a2-
capsular fibroblasts
c/m interstitium
pericytes
ureteric branching phenotype
increased stroma in nephrogenic zone
LIN28B overexpression delays nephron epithelialization, lobe formation, and a blastemal-like phenotype co-expressing CSC markers
Cited1/Aldh1a2 switch: the transitioning cell can commit to nephrogenesis, or remain uninduced
increased Aldh1a2+ stroma in nephrogenic zone, but Aldh1a2 is lost postnatally
ureteric bud tip cells remain embryonic in presence of NPC-like cells

Supplementary Fig. 1

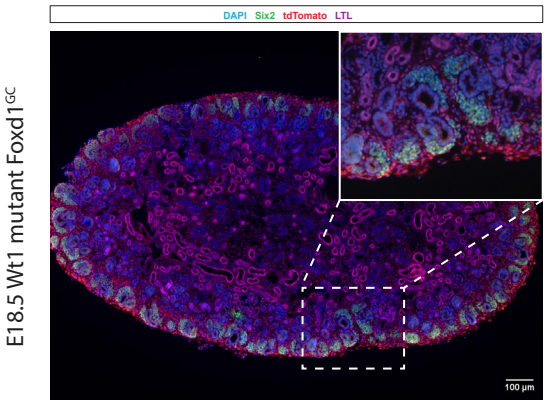

Supplementary Fig. 2

A.

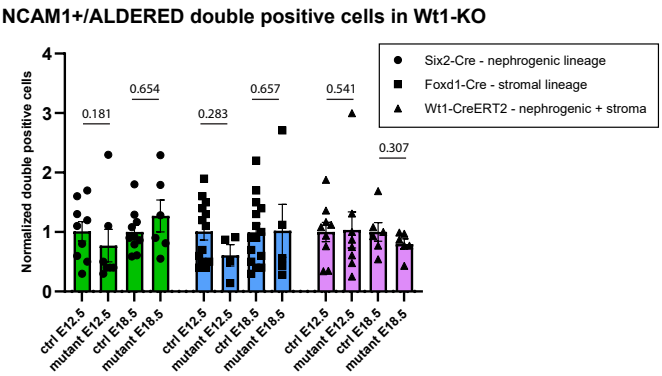

B.

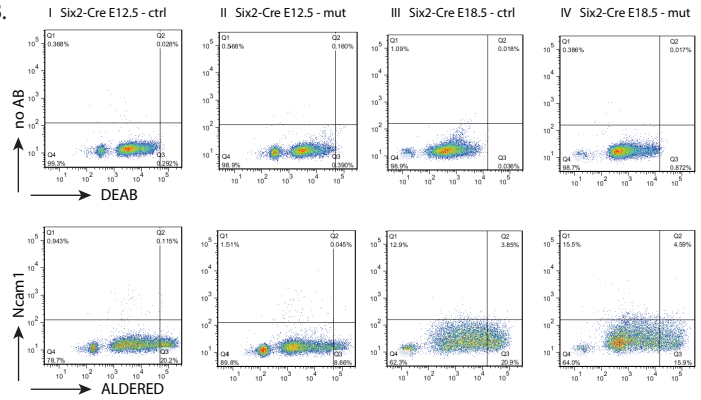

C.

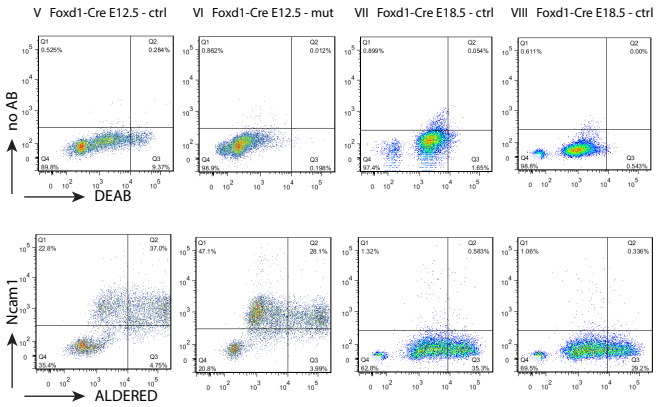

D.

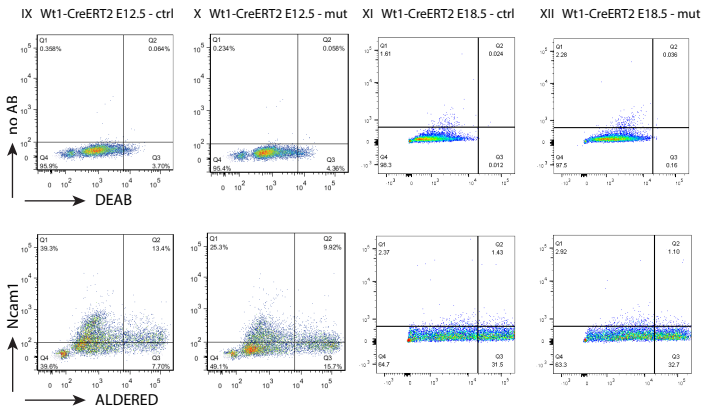

Supplementary Fig. 3

A.

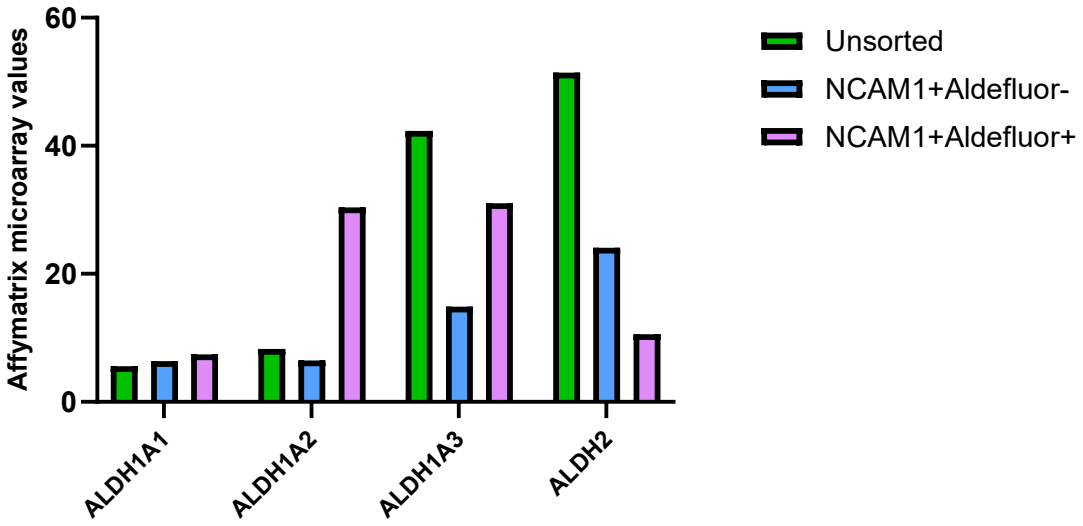

B.

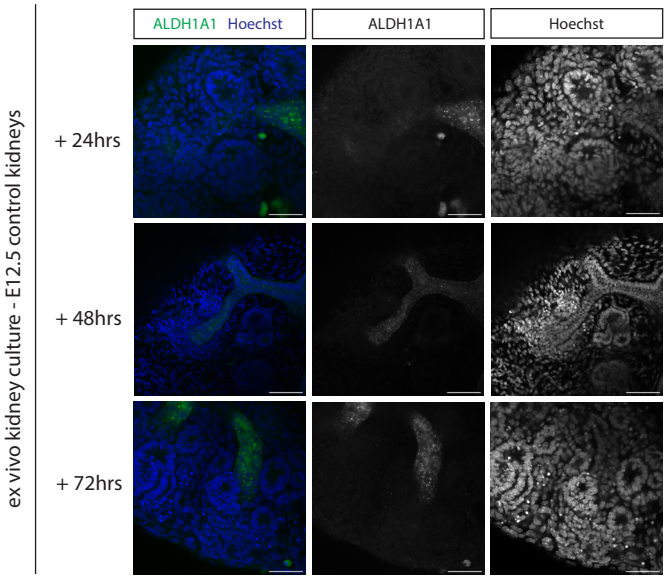

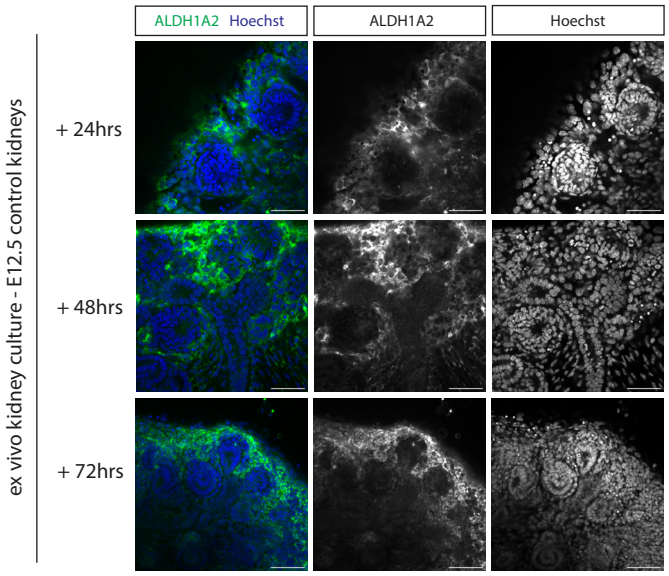

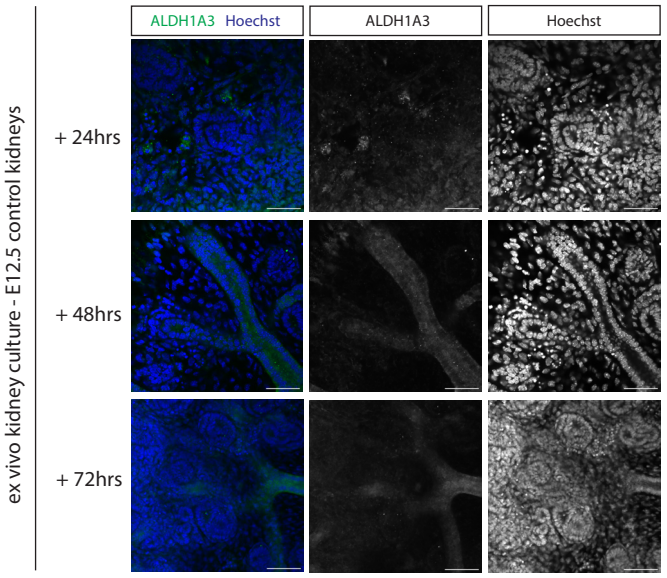

C.

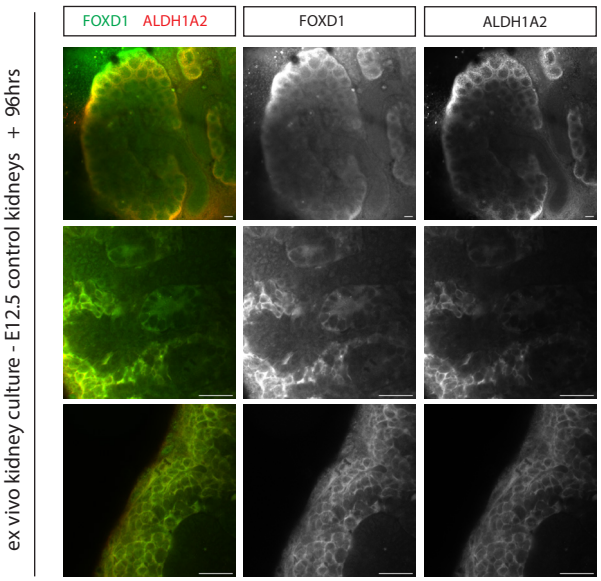

Supplementary Fig. 4

A.

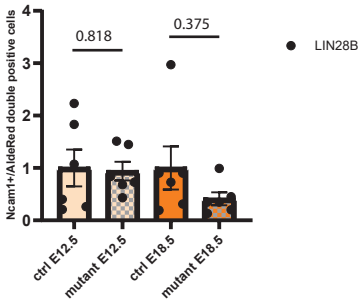

B.

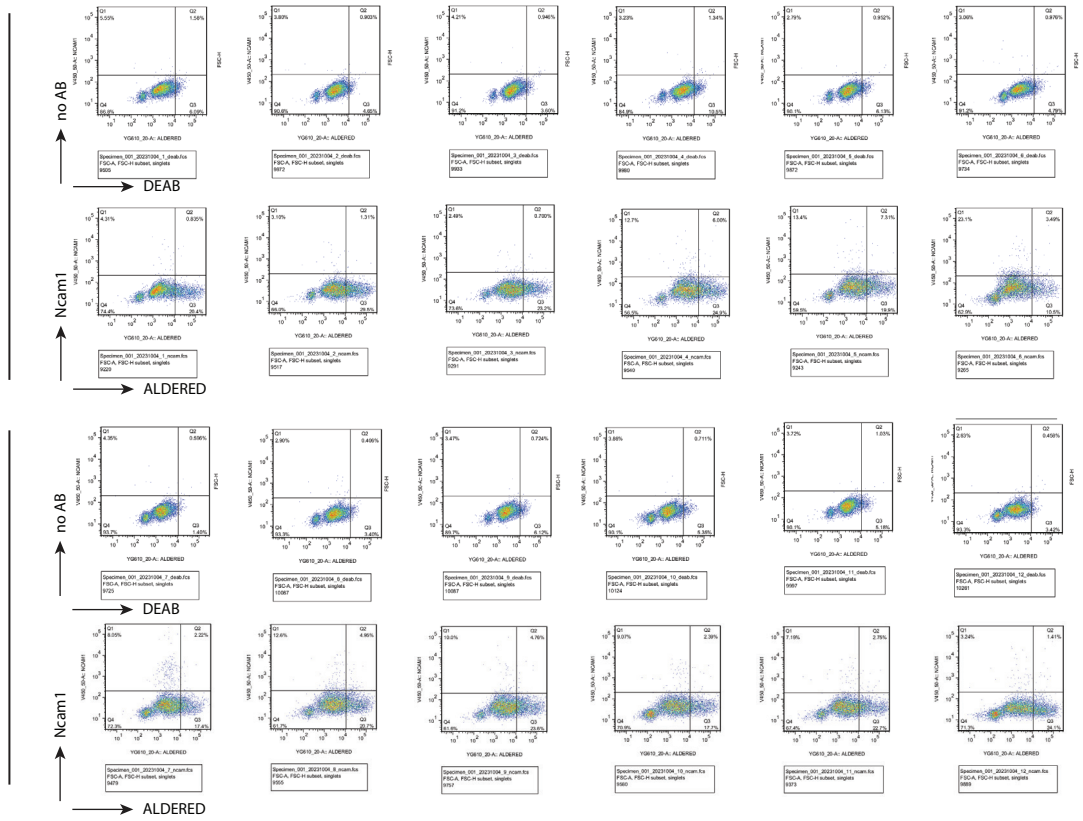

C.

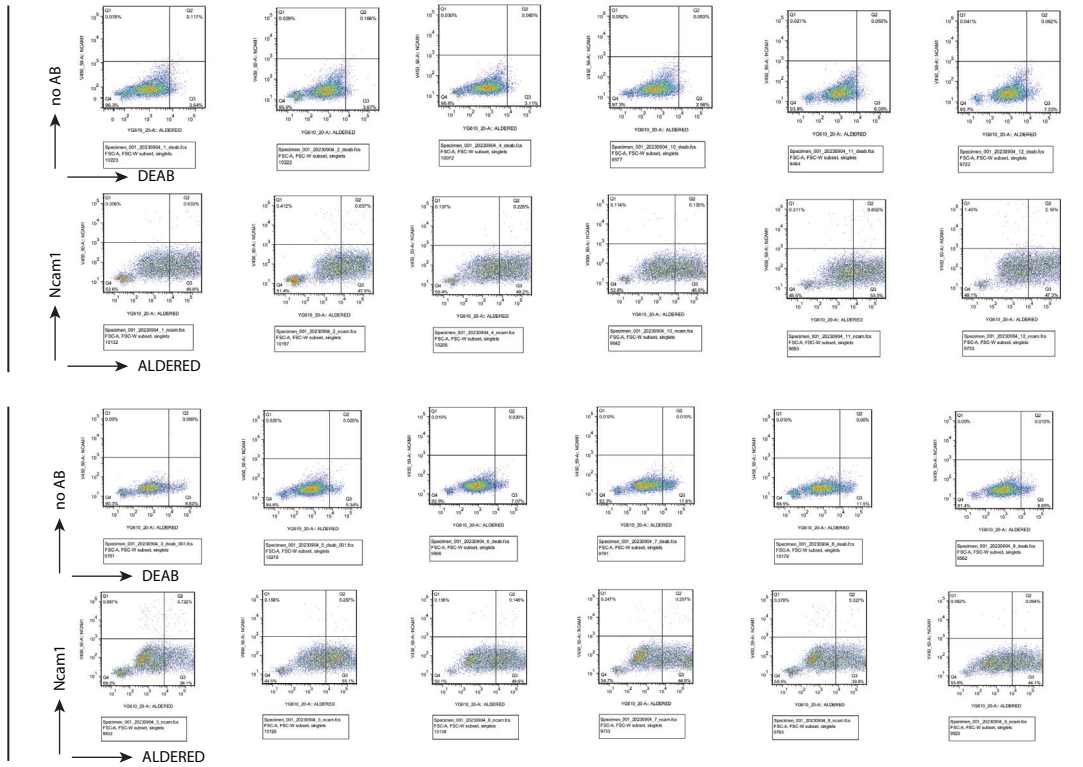
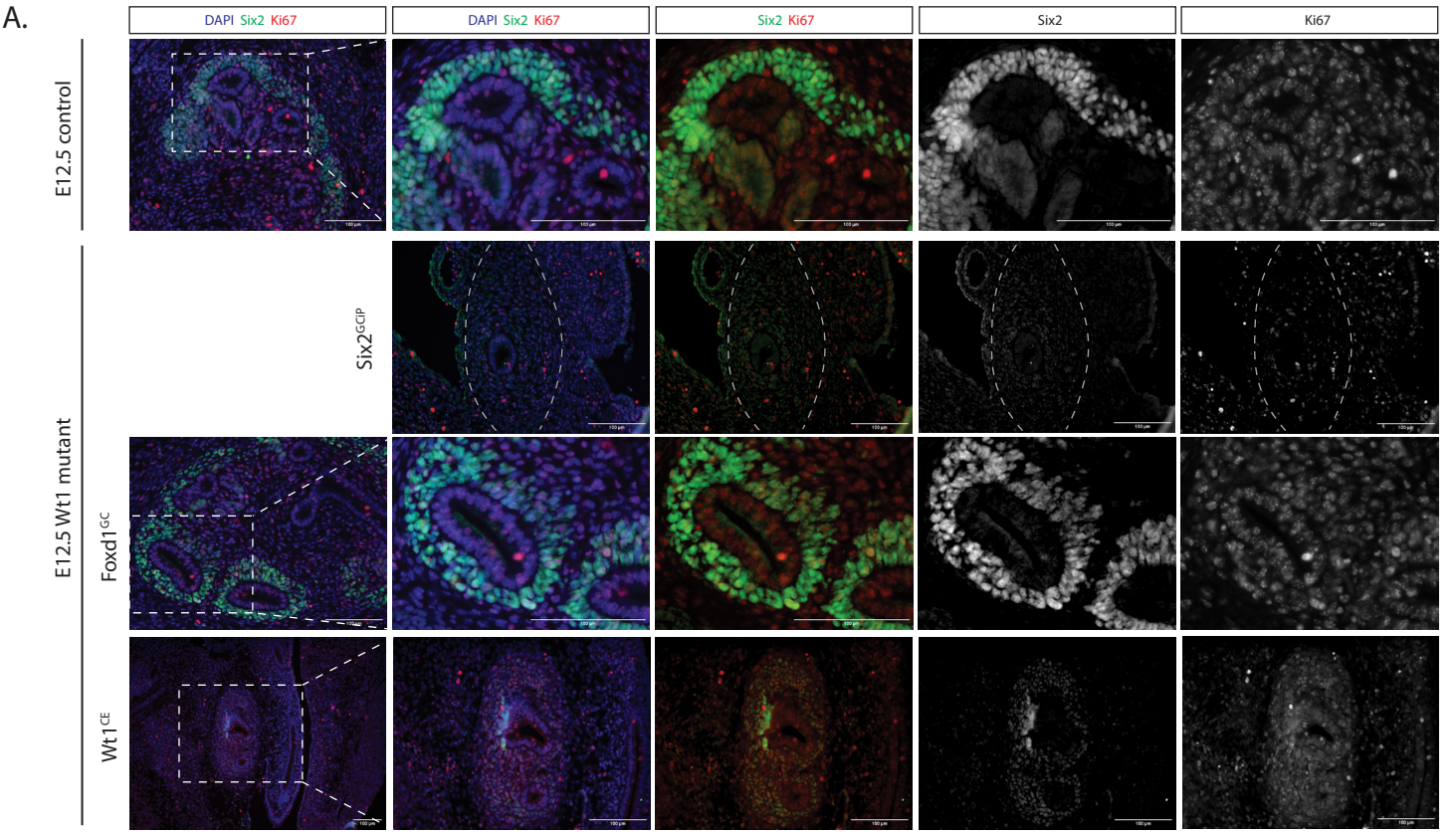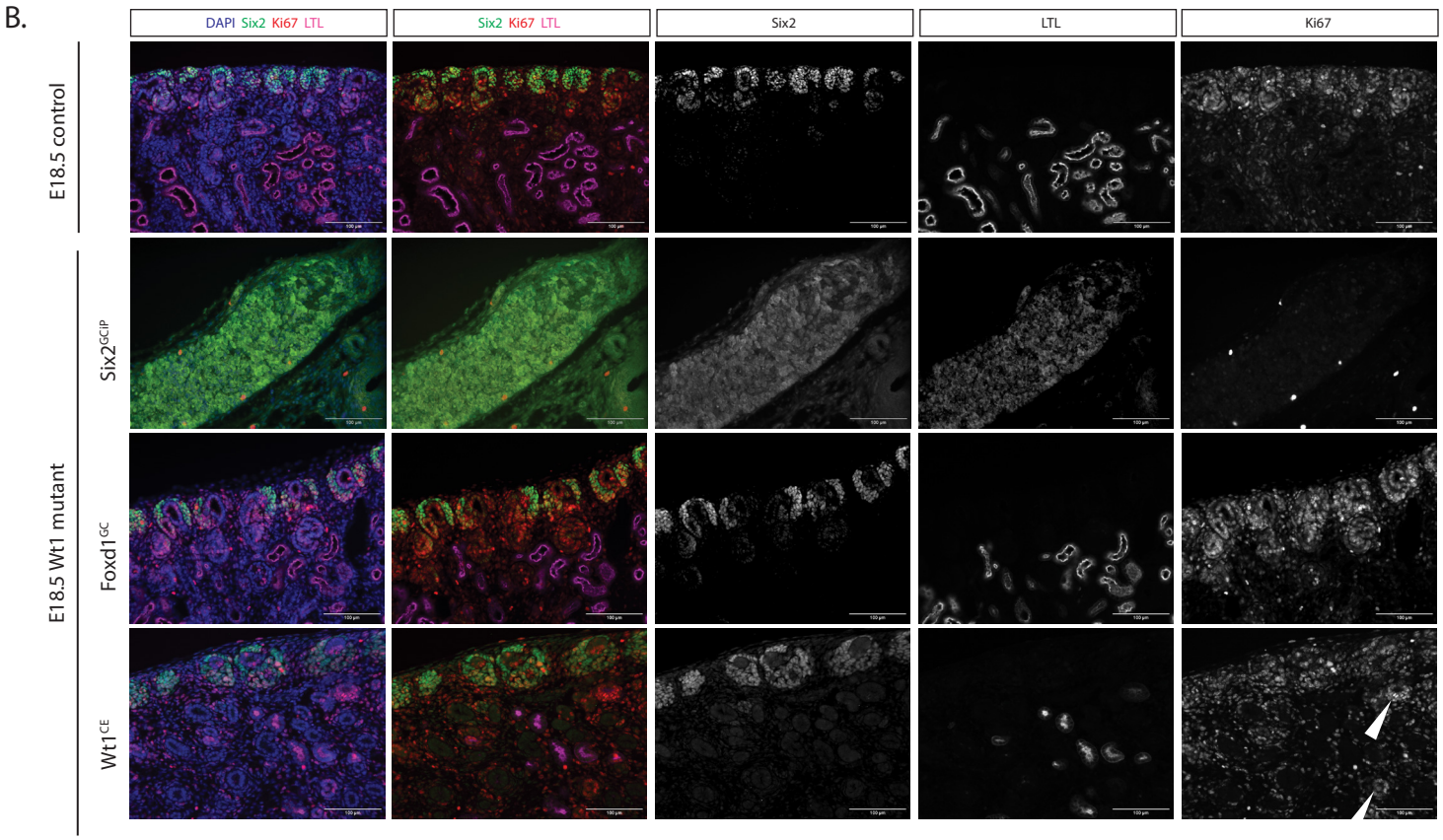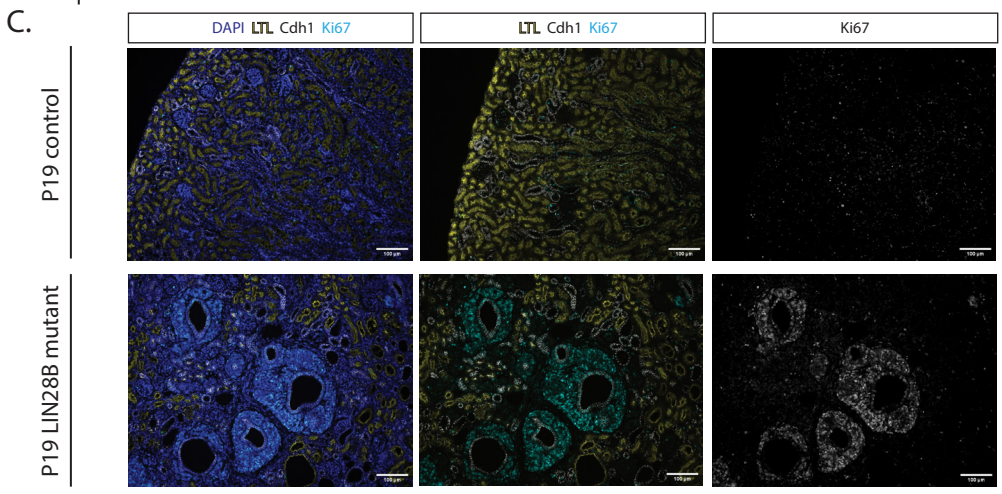
Supplementary Fig. 5